

Contents

Preface, xv

SECTION 1 ■ DETECTION AND APPROACHES TO LIVE CELL IMAGING, 1

- 1 Fluorescent Protein Tracking and Detection, 3
M.A. Rizzo, M.W. Davidson, and D.W. Piston
- 2 Constructing and Expressing Fluorescent Protein Fusions, 35
D.L. Spector and R.D. Goldman
- 3 Micropatterning Cell–Substrate Adhesions Using Linear Polyacrylamide as the Blocking Agent, 43
W.-h. Guo and Y.-l. Wang
- 4 CCD Cameras for Fluorescence Imaging of Living Cells, 53
W.C. Salmon and J.C. Waters
- 5 Fluorescence Perturbation Techniques to Study Mobility and Molecular Dynamics of Proteins in Live Cells: FRAP, Photoactivation, Photoconversion, and FLIP, 67
A. Bancaud, S. Huet, G. Rabut, and J. Ellenberg
- 6 Imaging Protein States in Cells, 95
H.E. Grecco and P.I.H. Bastiaens
- 7 A Versatile, Multicolor Total Internal Reflection Fluorescence and Spinning-Disk Confocal Microscope System for High-Resolution Live Cell Imaging, 119
W.D. Shin, R.S. Fischer, P. Kanchanawong, Y. Kim, J. Lim, K.A. Myers, Y. Nishimura, S.V. Plotnikov, I. Thievensen, D. Yarar, B. Sabass, and C.M. Waterman
- 8 Confocal Microscopy, Deconvolution, and Structured Illumination Methods, 139
J.M. Murray
- 9 Atomic-Force Microscopy for Biological Imaging and Mechanical Testing across Length Scales, 183
M. Plodinec, M. Loparic, and U. Aebi

viii ■ CONTENTS

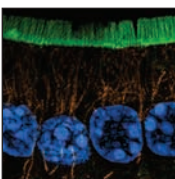
- 10 OMX: A New Platform for Multimodal, Multichannel Wide-Field Imaging, 203
I.M. Dobbie, E. King, R.M. Parton, P.M. Carlton, J.W. Sedat, J.R. Swedlow, and I. Davis
- 11 Digital Scanned Laser Light Sheet Fluorescence Microscopy, 215
P.J. Keller and E.H.K. Stelzer
- 12 First Steps for Fluorescence Correlation Spectroscopy of Living Cells, 229
M. Kinjo, H. Sakata, and S. Mikuni
- 13 Tracking and Quantitative Analysis of Dynamic Movements of Cells and Particles, 239
K. Rohr, W.J. Godinez, N. Harder, S. Wörz, J. Mattes, W. Tvaruskó, and R. Eils
- 14 Imaging Techniques for Measuring the Materials Properties of Cells, 257
K.E. Kasza, D. Vader, S. Köster, N. Wang, and D.A. Weitz
- 15 Computational Image Analysis of Cellular Dynamics: A Case Study Based on Particle Tracking, 271
K. Jaqaman and G. Danuser
- 16 Software Tools, Data Structures, and Interfaces for Microscope Imaging, 283
N. Stuurman and J.R. Swedlow
- 17 High-Throughput Microscopy Using Live Mammalian Cells, 297
S. Terjung, T. Walter, A. Seitz, B. Neumann, R. Pepperkok, and J. Ellenberg

SECTION 2 ■ IMAGING OF LIVE CELLS AND ORGANISMS, 315

- 18 In Vivo Imaging of Mammalian Cells, 317
J.R. Swedlow, I.M. Porter, M. Posch, and S. Swift
- 19 Live Cell Imaging of Yeast, 333
D.R. Rines, D. Thomann, J.F. Dorn, P. Goodwin, and P.K. Sorger
- 20 Live Imaging of *Caenorhabditis elegans*, 351
B. Podbilewicz and Y. Gruenbaum
- 21 Live Cell Imaging of Plants, 371
Y. Fang and D.L. Spector
- 22 Pushing the Limits of Live Cell Imaging in *Drosophila*, 387
R.M. Parton, A.M. Vallés, I.M. Dobbie, and I. Davis
- 23 Dynamic, Long-Term, In Vivo Imaging of Tumor–Stroma Interactions in Mouse Models of Breast Cancer Using Spinning-Disk Confocal Microscopy, 419
A.J. Ewald, Z. Werb, and M. Egeblad
- 24 High-Resolution Multiphoton Imaging of Tumors In Vivo, 441
J. Wyckoff, B. Gligorijevic, D. Entenberg, J. Segall, and J. Condeelis

- 25 Correlated Live Cell Light and Electron Microscopy Using Tetracysteine Tags and Biarsenicals, 463
G.M. Gaietta, T.J. Deerinck, and M.H. Ellisman
- 26 Intravital Microscopy of Normal and Diseased Tissues in the Mouse, 475
R.K. Jain, L.L. Munn, and D. Fukumura
- 27 Imaging Lipids in Living Cells, 523
C. Schultz, A.B. Neef, T.W. Gadella, Jr., and J. Goedhart
- 28 Development of Mammalian Cell Lines with *lac* Operator–Tagged Chromosomes, 541
Y.G. Strukov, M. Plutz, and A.S. Belmont
- 29 Imaging Gene Expression in Living Cells, 565
S.M. Janicki and D.L. Spector
- 30 Studying Mitosis in Cultured Mammalian Cells, 571
P. Wadsworth
- 31 Imaging Intermediate Filament Proteins in Living Cells, 583
E.R. Kuczmarski, T. Shimi, and R.D. Goldman
- 32 Methods for Expressing and Analyzing GFP-Tubulin and GFP-Microtubule-Associated Proteins, 605
H.V. Goodson, J.S. Dzurisin, and P. Wadsworth
- 33 Imaging of Membrane Systems and Membrane Traffic in Living Cells, 623
E.L. Snapp and P. Lajoie
- 34 Imaging Live Cells under Mechanical Stress, 641
B.P. Helmke and P.F. Davies
- 35 Imaging Single Molecules Using Total Internal Reflection Fluorescence Microscopy, 659
S.L. Reck-Peterson, N.D. Derr, and N. Stuurman
- 36 Cellular Imaging Using Total Internal Reflection Fluorescence Microscopy, 675
D. Toomre
- 37 Visualization and Quantification of Single RNA Molecules in Living Cells, 697
Y. Shav-Tal, S.M. Shenoy, and R.H. Singer
- Appendix: Cautions, 713
- Index, 721

CHAPTER TEN



OMX: A New Platform for Multimodal, Multichannel Wide-Field Imaging

Ian M. Dobbie,^{1,4} Emma King,^{2,4} Richard M. Parton,¹ Peter M. Carlton,³
John W. Sedat,³ Jason R. Swedlow,² and Ilan Davis¹

¹Department of Biochemistry, The University of Oxford, Oxford OX1 3QU, United Kingdom; ²Wellcome Trust Centre for Gene Regulation and Expression, College of Life Sciences, University of Dundee, Dundee DD1 5EH, United Kingdom; ³Department of Biochemistry and Biophysics, University of California, San Francisco, San Francisco, California 94143-2240

BIOIMAGING IS CURRENTLY UNDERGOING AN EXCITING revolution. This includes all aspects of imaging from probe development, specimen preparation, and instrumentation to image analysis and quantitation. Perhaps the most exciting developments are new platforms for imaging that radically advance the capabilities for collecting high spatial and high temporal resolution data. In many cases, the standard microscope has been replaced with new purpose-built platforms that are much more flexible and enable the implementation of new imaging modalities such as particular single-molecule and super-resolution imaging methods.

For live cell imaging, there are a number of competing critical requirements. Any live cell imaging system must be physically stable so that vibrations and temperature shifts do not move the sample or the optical path. This requirement is undermined by the need to change focus and to collect images as rapidly as possible. Fast live cell imaging thus requires a very stable, rapidly, and accurately moving imaging system with little vibration or temperature change. Photobleaching and photo-damage limit the photon budget, the number of photons transmitted through the microscope. When working at photon-limited levels, any additional sources of background and noise, such as stray light or noise from camera electronics, must be avoided. A recent study has highlighted the presence of additional non-Poisson noise in all tested commercial imaging platforms (Murray et al. 2007). Thus, photon-limited imaging is extremely challenging on traditional microscope platforms.

In this chapter, we discuss the design principles and applications of the OMX microscope, a new platform that provides unprecedented mechanical and thermal stabilities coupled with a photon budget that is dramatically improved over traditional microscope platforms. These characteristics make the OMX microscope outstanding for fast live cell imaging and super-resolution imaging. Moreover, its open flexible architecture makes it particularly amenable to adding other modes of microscopy to the platform.

HISTORY AND DESIGN OF OMX

OMX was designed and built by John Sedat in collaboration with David Agard (both at the University of California, San Francisco [UCSF]) and a number of coworkers including Mats

⁴Joint first authors.

Gustafsson (now at Janelia Farm Research Center), Lukman Winoto, and Peter Carlton. The microscope's name is derived from the original name that Agard and Sedat gave to their first wide-field deconvolution microscope, Optical Microscope 0 (OM0). OM0 was based on a Zeiss Axiomat, with an LN₂-cooled charge-coupled device (CCD) camera from Texas Instruments, and was run from a VAX 8650 mainframe computer. OM0 was used to acquire the first three-dimensional (3D) fluorescence images of cellular structures (Agard and Sedat 1983). There followed OM1, a turnkey, Silicon Graphics, Inc., workstation-controlled microscope that included fiber-optic illumination and stage-based focusing on an inverted microscope, and this provided some of the first 3D fluorescence images of living cells passing through the cell cycle (Minden et al. 1989). This was later commercialized as the DeltaVision microscope (Applied Precision, Inc. [API]), which continued its own path of development. The X in OMX stands for “eXperimental,” as the microscope is a continuously evolving platform that allows further development and improvement.

Traditional microscope stands have to take into account optical performance, cost, and ease of use. The optical path is designed to accommodate a range of additional components as well as the microscopist sitting at the microscope using the eyepieces and controls. Consequently, the efficiency of light transmission and the suppression of stray light are compromised. Additionally, it is difficult to rapidly and efficiently capture two channels simultaneously in wide-field microscopes, and capturing three or four channels simultaneously is nearly impossible. Although laser-scanning confocals can often capture multiple channels simultaneously, they are relatively slow, taking seconds to minutes per image stack, and have much lower photoefficiency (Murray et al. 2007). OMX was designed and built to provide a flexible platform that would be a foundation for many different modes of microscopy and to reduce the limitations found in conventional microscope platforms.

OMX includes separate modules for illumination, imaging, microscope control, and locating the sample. The layout and individual components are shown in Figure 1. For illumination, OMX uses solid-state continuous-wave lasers to provide bright monochromatic illumination. At least five separate lasers can be installed in the laser bed. Shuttering is achieved using individual solenoids that can operate reliably down to 1-msec opening time, and six-position wheels carrying neutral-density filters provide attenuation to control the excitation light intensity very precisely. At any time, all active lasers are focused into one of two fibers that provide alternative light paths into the microscope body. In the current implementation of OMX, one path is used for fast live cell imaging using conventional optics, and the other is used for three-dimensional structured illumination microscopy (3D-SIM). As described below, the flexible open design of OMX allows many alternative configurations.

The microscope is based on a solid-metal-block platform drilled to allow fitting of components. The block holds a kinematically mounted drawer that contains the elements of the fluorescence light path. This base is mounted on an antivibration table, and the whole assembly is housed in an acoustically isolated thermally controlled room. For fluorescence, the light path has been optimized to collect emission light, somewhat at the expense of excitation light. This block-and-drawer configuration replaces the standard microscope stand. The stage and lens mounting are made of Invar, a nickel–steel alloy with a very low coefficient of thermal expansion. Instead of using a rotating turret with a focus knob to raise, lower, and quickly change objectives, OMX objectives are fixed into kinematically mounted Invar plates adding stability and reproducibility. Focus change for optical sectioning is achieved by a piezoelectric device that changes the position of the stage and sample while leaving the lens fixed in place. Two Nanomover motors (Melles Griot) are used for translation in the image plane. There are no binoculars, and the microscope is kept isolated from the user in a filtered temperature-regulated environment. Up to four separate cameras can be mounted on OMX enabling fast and simultaneous multichannel data acquisition.

The fluorescence drawer used in OMX contains four beam splitters (BS1–4) that direct emitted light to the cameras (Fig. 1). The central beam splitters (BS1 and BS2) permit all wavelengths of excitation light to pass through virtually unreflected; the very small amount of reflected light

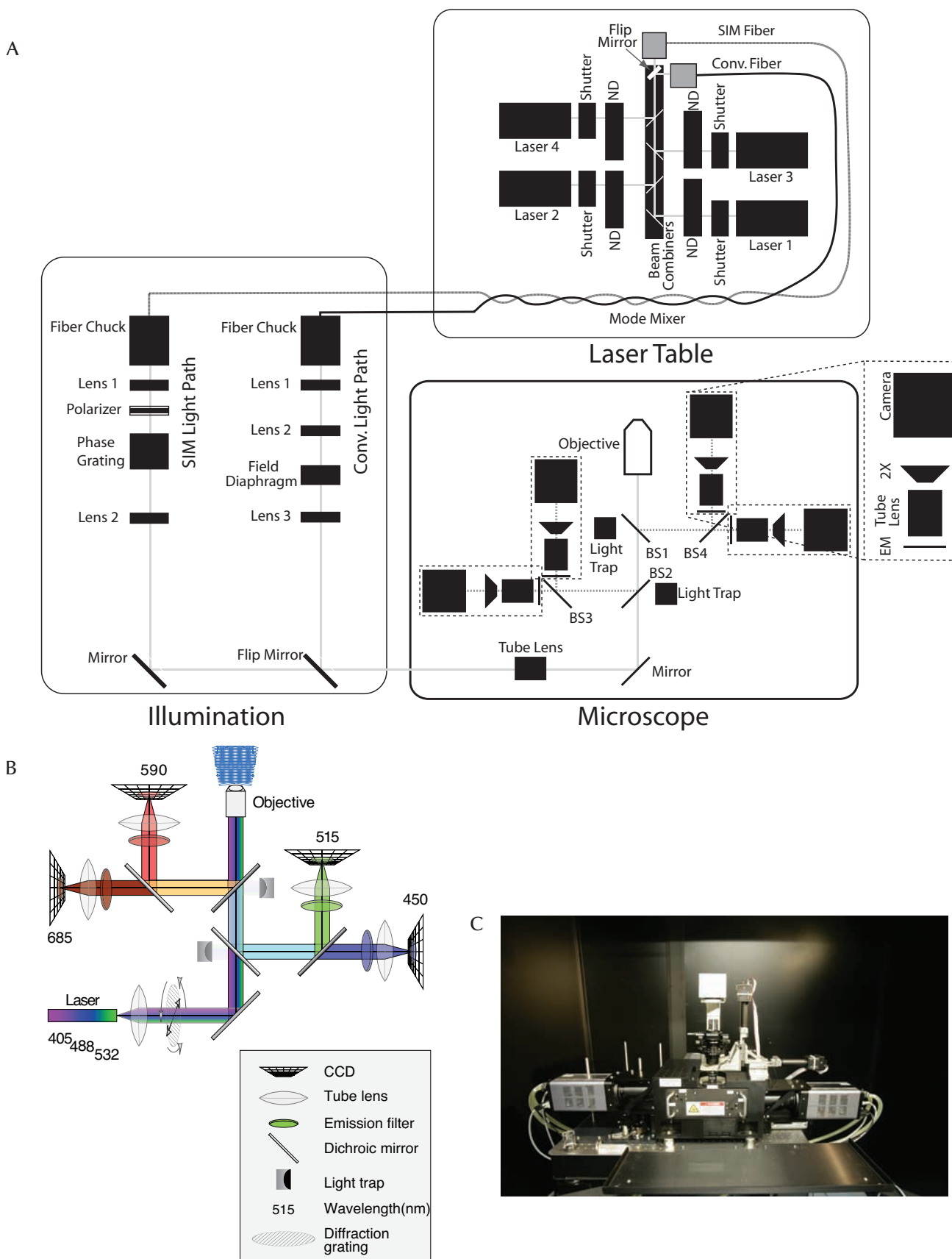


FIGURE 1. OMX components and layout. (A) Schematic of the optical setup of OMX. (B) The light path for the live cell drawer configuration to enable the use of simultaneous imaging of fluorescent combinations including CFP/YFP, GFP/mCherry, and CFP/YFP/mCherry. (C) A photograph of the OMX microscope body. (A, Courtesy of Paul Goodwin, API. B, © 2008 American Association for the Advancement of Science. Used by permission.)

is blocked by light traps suppressing stray light and, hence, reducing background. Emission light returning from the sample is reflected by the beam splitters to the appropriate cameras. First, both red and far-red light are reflected by BS2 to the left, where BS3 reflects red light to one camera and allows far-red light to pass through to another. Green and blue light pass through BS2, but both are reflected by BS1 to BS4, which directs green light to one camera and allows blue light to pass through. Drawers containing different beam-splitter arrangements may be easily switched in and out to allow simultaneous imaging of various combinations of fluorophores. Multiple cameras and a simply exchanged filter assembly allow the emitted light to be split in other ways such as by polarization.

OMX is controlled by a group of Windows-based computers that provide all user interfaces and control of the cameras, shutters, and other devices. The software controlling the system is written in C++ and Python. The Python source code is directly accessible on the computer during active operation and can be modified and reloaded at will. Users can issue commands or create new scripts via the built-in Python interpreter to control operation of the microscope at many levels, at any degree of sophistication desired. This flexibility allows complex illumination strategies such as those required for PALM-type experiments to be easily implemented. All functions running on auxiliary computers are accessible from the main control computer over the network via the Pyro distributed-object system (<http://pyro.sourceforge.net/>). Most user actions are saved to logs, so imaging sessions can be exactly recreated or debugged in case of problems. Furthermore, the temperature of the stage, the microscope body, the motors, and the entire room is continuously monitored and saved to disk, so users are aware of any possible irregularities.

To make sample finding and setup easy, the OMX uses a dedicated conventional auxiliary microscope, the low-magnification microscope (LMX). The LMX has a range of high-working-distance objectives with both transmission and epifluorescence illumination. The LMX has a high-precision motorized stage used for sample location and mapping. This stage is cross-indexed to the OMX stage to allow sharing of coordinates between the two systems. The LMX is configured to enable tile scanning of the entire region of a conventional slide that is within the stage travel of OMX. This tile scan can then be exported to the OMX control computer and used as a location map for finding specific features or locations once the slide has been mounted on OMX.

The workflow for using OMX for fixed samples involves preparing the samples, imaging them first on the LMX using a tile-scan mode in either bright field or fluorescence, and then moving the sample to the OMX stage. The tile scan is transferred to the OMX control computer, and the OMX software is used to locate regions for further imaging. For live cells, a prescan can be performed on the LMX and then used as a basis for finding living cells, or the live cell chamber can be directly mounted on OMX and then scanned using the OMX control software. The tile scan is displayed on the screen using texture mapping, allowing very fast panning and zooming over an entire slide's worth of image data at high resolution. This arrangement allows the operator to scan the slide at leisure without either illuminating the sample or needing to use eyepieces.

The first OMX prototype, OMX v1, was designed and built in John Sedat's laboratory at UCSF. API has licensed the OMX design and has built a number of beta systems referred to collectively as OMX v2. The data in Figures 2–6 are from two OMX v2 systems based at the Universities of Oxford and Dundee.

IMAGING APPLICATIONS USING OMX

The first versions of OMX have been outfitted for two specific applications: fast multichannel microscopy for high sensitivity and high temporal resolution analysis of living cells and 3D-SIM for high spatial resolution imaging of fixed cells. In the next sections, we detail the use of these different modes and show examples of the results that can be achieved.

Fast Live Imaging for High Temporal Resolution Analysis

Biological processes operate on a wide range of timescales from submillisecond to many minutes. The drive to develop mathematical models of molecular interactions presumes the availability of high-quality data sets that properly sample these events. Currently, conventional microscopes can record many single images per second. However, when sampling across space (optical sections) and spectral range (as in multichannel fluorescence microscopy), the practical limit of temporal sampling is on the order of ~ 1 3D image/sec. Any process that occurs on a subsecond timescale is thus subject to temporal aliasing. Furthermore, the raw speed of time-lapse acquisition is not necessarily the key parameter to consider because the efficiency of light transmission and detection determine critically whether useful images can be acquired in any particular set of conditions.

OMX offers two distinct advantages for live cell imaging. First, up to four channels can be recorded simultaneously, or in the case of fluorophores with some spectral overlap, in very rapid sequence such that the delay between sampling at different wavelengths is no more than 1–2 msec. Second, the very bright laser-light sources, fast shutter, rapid and stable focusing, and integration of electronic control mean that very rapid, accurate, and precise 3D imaging is achievable. The current implementations of OMX can record 2–10 3D images/sec for each channel. The fastest we have run our microscopes, with 1-msec exposure, is 93 or 107 images/sec depending on the precise individual prototype. The major speed bottleneck is the read time of the cameras, which for a full-frame image (512×512 -pixels, 10 MHz, 16 bits) is 13 msec. Reducing the imaging area on the CCD substantially reduces this time.

Most live cell imaging applications make use of fluorescent proteins (FPs). The choice of FP is dependent on the laser lines present on the system and on the brightness and photostability of the proteins. For simultaneous acquisition of multiple wavelengths, well spectrally separated FPs work best. For example, green fluorescent protein (GFP) and mCherry are compatible with the 488 nm and 593 nm laser lines, do not spectrally overlap significantly, and are relatively photostable. Figures 2 and 3 show examples of using this mode of imaging FP-labeled living yeast, *Drosophila*, and human cells

To date, OMX uses the Bioprotech FCS2 closed live cell chamber. Samples are grown on or adhered to 40-mm circular (no. 1.5 thickness) coverslips either by their own adherent properties or by coating slides with substances such as polylysine or concanavalin A. The design of the FCS2 system permits temperature control and media exchange but not an environment in which CO_2 is regulated. A critical advance for the future is the design and building of an environmental chamber for live cell imaging.

3D-SIM for High Spatial Resolution Analysis

The achievable resolution in light microscopy has been limited to $\sim \lambda/2$ by diffraction since the development of the modern microscope in the late 1800s. Over the past few years, a number of methods for overcoming this diffraction limit have been developed. These methods are collectively known as super-resolution techniques (Hell 2009).

3D-SIM uses structure within the illumination and multiple images per sample section combined with postacquisition analysis to double the achievable resolution in all three spatial dimensions. By illuminating a fluorescent sample with a sinusoidal striped pattern, additional information from the sample is encoded in the fluorescent emissions (Gustafsson 2000; Schermelleh et al. 2008). The phase of the striped pattern is shifted over a full cycle in five steps and also rotated to three positions at 60° intervals. The resulting 15 images per z section are processed to produce the final super-resolution image. Images of fluorescent beads in both conventional wide-field microscopy and 3D-SIM, with profiles showing the resolution improvement, are shown in

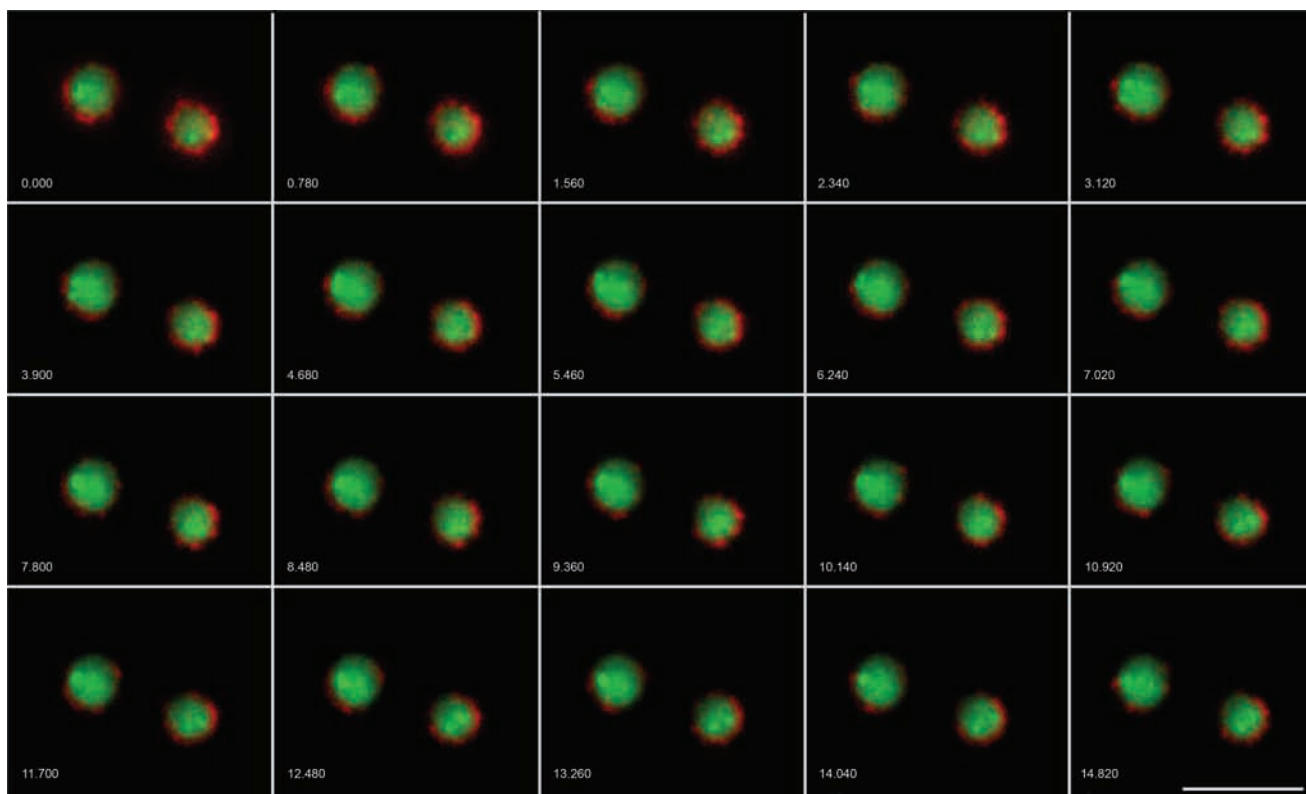


FIGURE 2. Live cell imaging with OMX showing *Saccharomyces cerevisiae* with mCherry-labeled nuclear pore complexes and GFP-TetO-tagged chromosome IV (13 z sections, 0.3 μm apart, time lapse 780 msec). Wavelengths were acquired simultaneously on OMX v2 and then aligned and fused. The images have been deconvolved, and the maximum intensity is projected. Numbers indicate elapsed time in seconds. Scale bar, 5 μm . (Courtesy of Emma King and David Dickerson, University of Dundee, and Paul Goodwin, API.)

Figure 4. The achievable resolution varies from 105 nm with 405 nm illumination to 165 nm with 593 nm resolution (Gustafsson 2000).

As implemented on the current versions of OMX, 3D-SIM is realistically useful for fixed specimens. With that caveat, 3D-SIM on OMX has been successfully applied to a broad range of specimens—microorganisms, vertebrate cells, tissue sections, and even whole embryos. Our own microscopes have been used by a variety of collaborators, and these data will be published elsewhere. Figures 5 and 6 show two examples of the application of OMX in cultured *Drosophila* macrophages and HeLa cells (Fig. 5) and a section of fixed mouse colon (Fig. 6). The improvement in axial resolution in comparison with conventional deconvolution or confocal imaging is apparent in the subcellular structures visible in these images. For example, the diameters of microtubule fibers are closer to their true sizes, and overlapping and dense fields of microtubules or actin networks can be resolved into individual fibers much more readily.

Sample Preparation and Imaging Protocols for 3D-SIM

Sample preparation for imaging using the structured illumination (SI) protocol on OMX does not vary greatly from that used for image acquisition on other systems. However, emphasis needs to be placed on good practice to ensure a specific, bright, and photostable fluorescent signal as well as good morphological preservation. Fixation should be of the highest quality that is consistent with preserving epitopes and the fluorescence of FPs as appropriate.

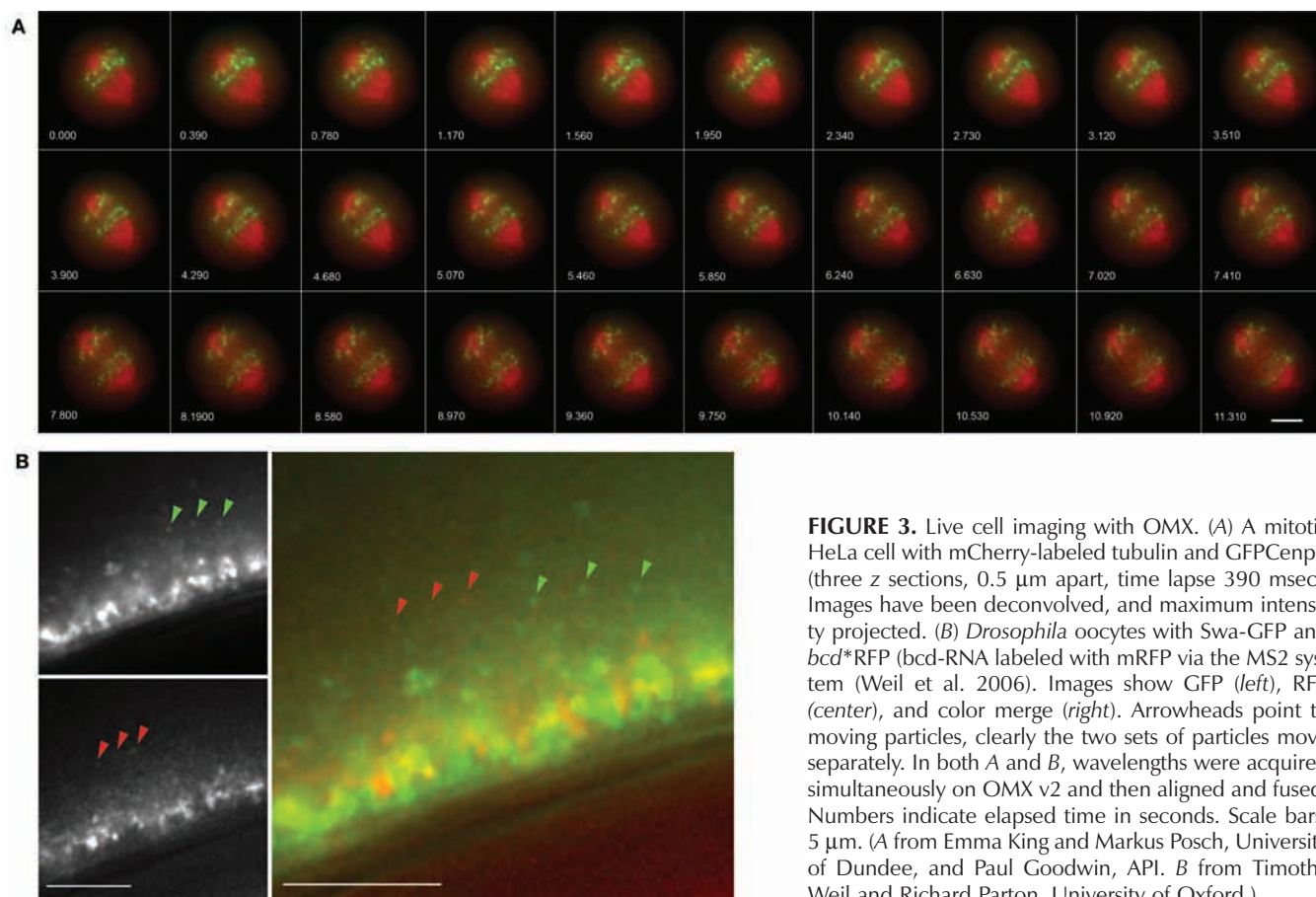


FIGURE 3. Live cell imaging with OMX. (A) A mitotic HeLa cell with mCherry-labeled tubulin and GFPcenpB (three z sections, 0.5 μm apart, time lapse 390 msec). Images have been deconvolved, and maximum intensity projected. (B) *Drosophila* oocytes with Swa-GFP and *bcd**RFP (*bcd*-RNA labeled with mRFP via the MS2 system (Weil et al. 2006). Images show GFP (left), RFP (center), and color merge (right). Arrowheads point to moving particles, clearly the two sets of particles move separately. In both A and B, wavelengths were acquired simultaneously on OMX v2 and then aligned and fused. Numbers indicate elapsed time in seconds. Scale bars, 5 μm . (A from Emma King and Markus Posch, University of Dundee, and Paul Goodwin, API. B from Timothy Weil and Richard Parton, University of Oxford.)

The system is designed for use with scrupulously clean no. 1.5 (0.17 mm thick) coverslips. So far the system has been used to image material within 16 μm of the surface of the coverslip. The fixation conditions and the choice of primary antibody (one that localizes strongly to the structure of interest) need to be optimized to achieve a good signal-to-background ratio, thus optimizing reconstruction output and minimizing the generation of reconstruction artifacts. A broad range of samples has been successfully imaged using the SI protocol of OMX—from cell monolayers to mouse-gut wax sections to plant-leaf peels.

There is a wide choice of bright photostable secondary antibodies to match the laser lines available on the system allowing excellent image quality by optimizing the match between the filter systems and the excitation and emission characteristics of the fluorochromes. We have successfully utilized Alexa Fluor-conjugated secondary antibodies (Invitrogen), and recently, Jackson ImmunoResearch, Inc. has released a new DyLight collection that further expands the availability of wavelength-specific antibodies to target a broader range of primary antibodies raised in different species. The 593 nm laser line is compatible with both 568 and 594 nm excitable dyes. Protein fusions of a bright FP, such as GFP, can be used for imaging samples that require a small number of z sections and/or exposure to a limited number of excitation wavelengths. However, the photostability of FPs has so far limited their use in 3D-SIM. Acquisition of images using the 3D-SIM protocol is possible using cameras with electron-multiplying CCD amplification enabled, which has opened the door to the imaging of dimmer samples with low background fluorescence. Furthermore, to protect the fluorescence emitted and to minimize

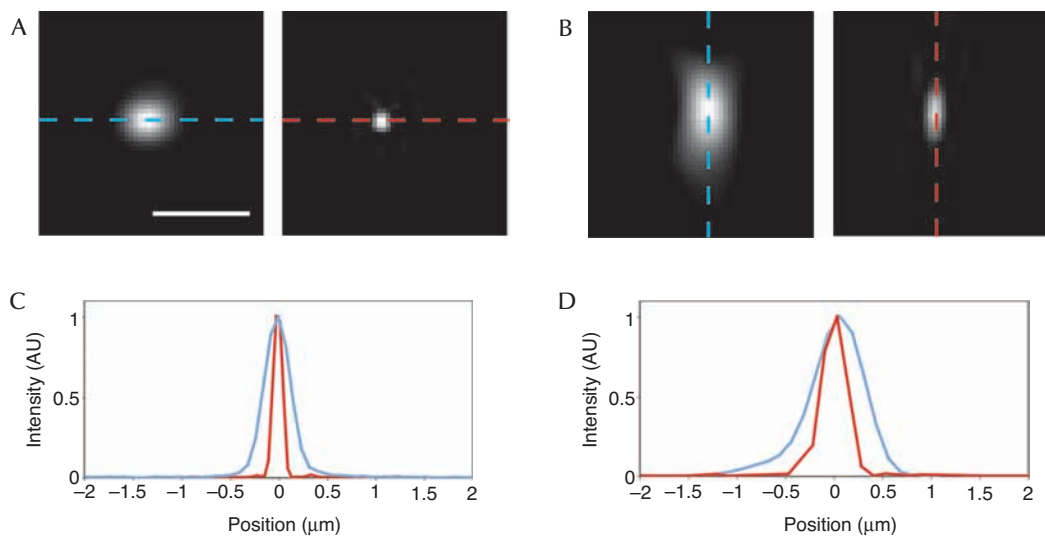


FIGURE 4. OMX point-spread functions with and without 3D-SIM. Images (A,B) and line scans (C,D) of 89-nm fluorescent beads illuminated at 488 nm and detected at 510 nm in conventional wide-field- and 3D-SIM-imaging modes. x-y (A) and x-z (B) are shown in conventional wide-field mode (left images) and in a 3D-SIM reconstruction (right images). Profiles through the center of a bead clearly show the increase in resolution between conventional wide-field microscopy (blue) and 3D-SIM (red), in both x-y (C) and z (D), demonstrating the increase in resolution is achieved in z as well as in x-y. Scale bar, 1 μm . (Courtesy of Ian Dobbie, University of Oxford.)

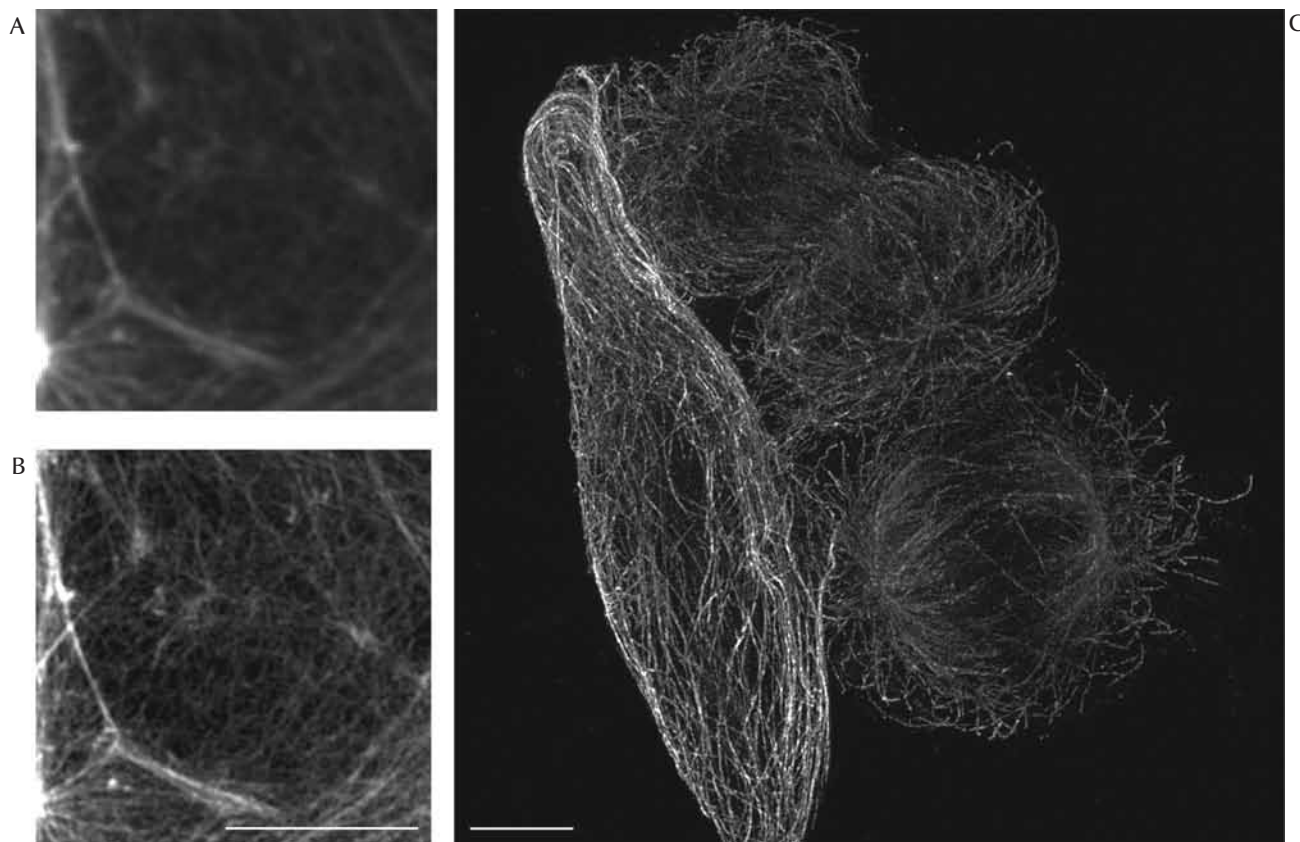


FIGURE 5. 3D-SIM imaging of cultured cells on OMX. *Drosophila* macrophage cells that have been fixed and stained for F-actin with fluorescein-isothiocyanate (FITC)-phalloidin are shown (A) in a conventional wide-field image and (B) in a 3D-SIM reconstruction; the latter clearly shows the dramatic increase in detail achieved. (C) A formaldehyde-fixed HeLa cell-stained antitubulin and an Alexa Fluor 488 secondary antibody are also shown; these images were acquired using the 3D-SIM protocol on OMX v2. For each panel, the image shown is a maximum-intensity projection through the full volume of the cells. Scale bars, 5 μm . (Parts A and B are from Ian Dobbie and Ilan Davis, University of Oxford. Part C is from Jason Swedlow, University of Dundee, and Paul Goodwin, API.)

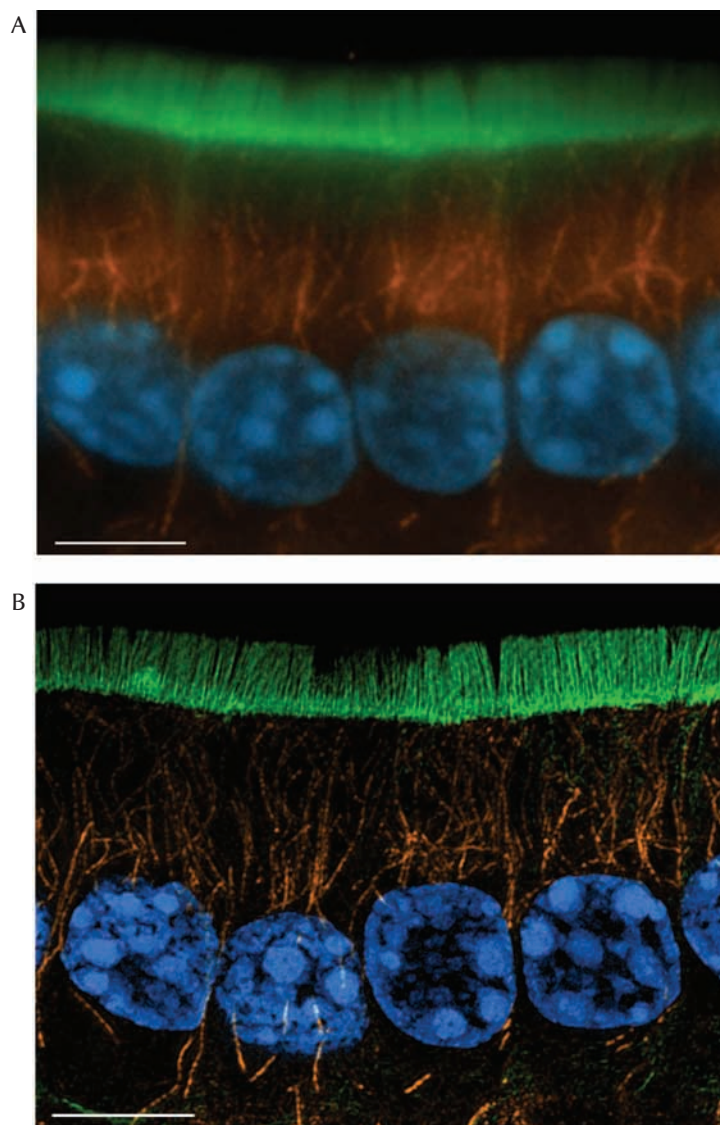


FIGURE 6. 3D-SIM imaging of cryosections on OMX. A 10- μm cryosection of formaldehyde-fixed mouse small intestine, stained with DAPI (4',6-diamidino-2-phenylindole) to show nuclei (blue), antitubulin/Alexa Fluor 568 to show microtubules (orange), and FITC-phalloidin to show F-actin (green), is shown as (A) a deconvolved conventional wide-field image with five z sections and maximum-intensity projection and as (B) an image acquired using the 3D-SIM protocol on an OMX v2. In B, the wavelengths were acquired sequentially, reconstructed, and then aligned and fused to form a five-z-section maximum intensity projection. Scale bars, 5 μm . (Courtesy of Emma King and Paul Appleton, University of Dundee.)

changes of refractive index in the light path, samples should be mounted in a medium that matches the refractive index of the objective lens fitted. The mountant should contain antifade agents such as 1,4-phenylenediamine in a buffer of 90% glycerol and 10% Tris; we have found this to give optimal results, especially with 594 nm excitable dyes.

FUTURE DIRECTIONS

OMX is fundamentally a research instrument and is still under development. Its basic premise of reworking the fluorescence light microscope from the ground up provides a very flexible new platform. Currently, the commercial OMX sold by API is set up for fast live multichannel imag-

ing and super-resolution 3D-SIM. Adding novel functionality is relatively easy because of the open nature of the excitation light paths and the flexibility of the hardware and software controls. Some of the possible extensions in functionality are discussed below, although this list is far from exhaustive and is continuously evolving.

Two-Dimensional SI Microscopy in Living Cells

3D-SIM on OMX is able to double the resolution compared with a conventional fluorescence microscope. However, there are two major drawbacks to the technique. To perform 3D SI, at least five illumination phases must be recorded at three different angles. Therefore, for each reconstructed image section, 15 images must be recorded. This can cause substantial photobleaching and very slow acquisition because of the large number of images required. Data collection is further slowed by the fact that the current implementation of OMX rotates a physical diffraction grating to take images with the SI at different angles. This process requires ~ 2 sec per angle change. To properly perform reconstructions to provide the higher-resolution output image, any structure of interest must not move during imaging by a significant fraction of the 100 nm resolution. In the current generation of OMX, the minimum time to take a full SI z series is ~ 10 sec, long enough for the internal contents of the cell to move substantially more than 100 nm. This situation can be improved in two complimentary ways. First, by providing z sectioning via total internal reflection fluorescence (TIRF), only a single z section is required, and the number of images that are captured is reduced to 9, three phases at three angles. It should be noted that this provides a single-section super-resolution image rather than a 3D-image stack. Second, using a spatial light modulator, the diffraction grating angle can be changed without physically moving the optical elements. Combining these two approaches allows single two-dimensional (2D) TIRF super-resolution images to be collected in <100 msec (Kner et al. 2009).

TIRF

TIRF is a method for achieving 100 nm z resolution combined with very low fluorescence background. This is achieved by illuminating the sample with light above the critical angle for complete reflection between the coverslip and the sample. This produces an evanescent wave parallel to the coverslip that falls exponentially with distance from the interface (see Chap. 36). Multiwavelength objective-based TIRF has been implemented on the Sedat laboratory OMX by redirecting the standard wide-field illumination into a multiwavelength single-mode fiber. This fiber is then translated to shift the position of the beam path in the back focal plane. This allows rapid changes of the angle of incidence to achieve TIRF at different wavelengths for multicolor live TIRF imaging.

3D TIRF

The precise control of the angle of incidence on OMX also allows the acquisition of TIRF images at a range of angles all above the critical angle. In this way, an image stack can be created by steadily imaging further into the sample. Image processing allows calculation of the depth of objects within the image with very high z resolution. This technique allows imaging with 100 nm z resolution to depths up to 1 μm .

Image Processing for Live Cell Imaging

A primary design aim of OMX is to maximize the signal-to-noise ratio (SNR) to gather as much data as possible from limited illumination intensity and short exposures that occur in fast imaging of highly photosensitive living cells. Analyzing the data generated in fast live imaging requires

the implementation of object identification and tracking software that can track rapidly moving particles in images with limited SNR (Jaqaman et al. 2008). These tools are critical for delivering quantitative measurements of objects recorded in live cell imaging (see Chaps. 13, 15, and 16).

A promising area for future improvement in fast live cell imaging is the use of image-processing tools to improve SNR and thus the performance of subsequent analysis tools. Deconvolution, used on 3D-data stacks from OMX, is able to improve the SNR using the point-spread function to develop an estimate of the in-focus object in the sample (Swedlow et al. 1997; Wallace et al. 2001; Parton and Davis 2006). In addition, the application of denoising algorithms can substantially improve the appearance of image data. Denoising relies upon the fact that signal but not noise is correlated between adjacent pixels in 2D or 3D. In 2D, denoising is relatively simple and widely applied using processes such as a Gaussian or a median filter. Extending this to 3D further improves the SNR because extra information is available. Recently, more advanced algorithms have become available. By applying denoising techniques to four-dimensional image sets, 3D data in time, even more SNR improvement can be gained.

Photoactivation Localization Microscopy

A second technique for generating so-called super-resolution images, with a precision >20 nm, is photoactivation localization microscopy (PALM) (Betzig et al. 2006). This technique works by iteratively building up an image from the fluorescence emission of individual dye molecules imaged in a stochastic manner, a small number at a time. Basic 2D PALM, as described above, can be achieved easily on OMX, as it simply requires a custom illumination pattern, low-intensity activation pulse, followed by multiple frames of standard excitation imaging. This can either bleach out the active molecules or be followed by a deactivation pulse. z -position information can be added to this by either taking images at two z positions (Juetten et al. 2008) or by using an imaging system with astigmatism (Huang et al. 2008). The multiple cameras and simple filter arrangement on OMX allow multiple z positions to be simultaneously acquired using a 50–50 beam splitter between the two channels and introducing an extra lens into one channel producing a focus shift relative to the other channel. Alternatively, astigmatism can be easily introduced by having a cylindrical lens in the illumination path. On OMX, this is easily achieved because of the open access to the illumination beam path.

CONCLUDING REMARKS

Because of its flexibility, the OMX platform is still rapidly evolving. We anticipate that many more functionalities will be added to the platform, as essentially all applications of wide-field fluorescence microscopy can be improved by taking advantage of the improved light budget, stability, and simultaneous acquisition characteristics of the system.

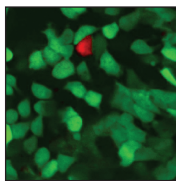
ACKNOWLEDGMENTS

We thank Sam Swift, Chris Allan, and Benny Chitambira for help in running the University of Dundee OMX; Paul Appleton, David Dickerson, Markus Posch (University of Dundee), and Paul Goodwin (API) for permission to use their figures in this chapter; Kim Nasmyth for discussions on the biological applications of OMX; and Tim Weil for his help acquiring swallow and bicoid time-lapse images. The purchase and use of the University of Dundee OMX microscope is supported by the Scottish University Life Sciences Alliance. Work in the Swedlow Laboratory using OMX is supported by the Wellcome Trust (067433), Cancer Research UK (C303/A5434), and the Biotechnology and Biological Sciences Research Council (BB/G01518X/1). I.D. and R.M.P. are

supported by a Senior Research Fellowship from the Wellcome Trust (081858) to I.D. OMX was purchased in Oxford with grants from the Wellcome Trust, E.P.A. Cephalosporin fund, and Oxford University Press Fell Funds.

REFERENCES

- Agard D, Sedat J. 1983. Three-dimensional architecture of a polytene nucleus. *Nature* **302**: 676–681.
- Betzig E, Patterson GH, Sougrat R, Lindwasser OW, Olenych S, Bonifacino JS, Davidson MW, Lippincott-Schwartz J, Hess HF. 2006. Imaging intracellular fluorescent proteins at nanometer resolution. *Science* **313**: 1642–1645.
- Gustafsson MG. 2000. Surpassing the lateral resolution limit by a factor of two using structured illumination microscopy. *J Microsc* **198**: 82–87.
- Hell SW. 2009. Microscopy and its focal switch. *Nat Methods* **6**: 24–32.
- Huang B, Wang W, Bates M, Zhuang X. 2008. Three-dimensional super-resolution imaging by stochastic optical reconstruction microscopy. *Science* **319**: 810–813.
- Jaqaman K, Loerke D, Mettlen M, Kuwata H, Grinstein S, Schmid SL, Danuser G. 2008. Robust single-particle tracking in live-cell time-lapse sequences. *Nat Methods* **5**: 695–702.
- Juette MF, Gould TJ, Lessard MD, Mlodzianoski MJ, Nagpure BS, Bennett BT, Hess ST, Bewersdorf J. 2008. Three-dimensional sub-100 nm resolution fluorescence microscopy of thick samples. *Nat Methods* **5**: 527–529.
- Kner P, Chhun BB, Griffis ER, Winoto L, Gustafsson MG. 2009. Super-resolution video microscopy of live cells by structured illumination. *Nat Methods* **6**: 339–342.
- Minden JS, Agard DA, Sedat JW, Alberts BM. 1989. Direct cell lineage analysis of *Drosophila melanogaster* by time-lapse, three-dimensional optical microscopy of living embryos. *J Cell Biol* **109**: 505–516.
- Murray JM, Appleton P, Swedlow JR, Waters JC. 2007. Evaluating performance in fluorescence 3-D microscopy. *J Microsc* **228**: 390–405.
- Parton R, Davis I. 2006. Lifting the fog: Image restoration by deconvolution. In *Cell biology* (ed. JE Celis), pp. 187–200. Academic, New York.
- Schermelleh L, Carlton PM, Haase S, Shao L, Winoto L, Kner P, Burke B, Cardoso MC, Agard DA, Gustafsson MGL, et al. 2008. Subdiffraction multicolor imaging of the nuclear periphery with 3D structured illumination microscopy. *Science* **320**: 1332–1336.
- Swedlow JR, Sedat JW, Agard DA. 1997. Deconvolution in optical microscopy. In *Deconvolution of images and spectra* (ed. PA Jansson), pp. 284–309. Academic, New York.
- Wallace W, Schaefer LH, Swedlow JR. 2001. A workingperson's guide to deconvolution in light microscopy. *BioTechniques* **31**: 1076–1097.
- Weil TT, Forrest KM, Gavis ER. 2006. Localization of bicoid mRNA in late oocytes is maintained by continual active transport. *Dev Cell* **11**: 251–262.



Index

A

- Abdominal window preparation in mice, 476, 477t, 494
- Acceptor photobleaching, 98–99, 99f, 108–110
- AcGFP, 612
- Acousto-optical tunable filters (AOTFs), 71, 75, 663, 681
- Actin, GFP-tagged, 36, 190–193, 190f
- Actin-depolymerizing drugs, 630
- Actin promoter, 36
- Activated sodium orthovanadate (recipe), 116
- Acute (exteriorized) tissue preparations, 477t, 478, 478f
- ADC (analog-to-digital converter), 341, 342
- Adhesions, micropatterning cell-substrate, 43–51
- Aequorea coerulescens* (jellyfish), 16
- Aequorea victoria* (jellyfish), 3
- Aequorin, 3, 6
- AFM. *See* Atomic force microscopy (AFM)
- Agard, David, 203
- Aggrecans, 187
- Agrobacterium tumefaciens*
preparation of competent cells, 376
transferring vectors into, 373, 381
- Air-curtain incubator, 577
- Airy disk, 141, 142, 143f, 173, 179, 335
- Aluminum fluoride, 630
- Analog-to-digital converter (ADC), 341, 342
- Anesthesia, 425, 436–438, 447, 448, 453, 459
- Antibody
for determination of protein fusion location, 40
for determination of protein fusion size, 41
labeling with fluorescent dyes, 103–105
- AOTFs (acousto-optical tunable filters), 71, 75, 663, 681
- APB. *See* Acceptor photobleaching
- APD (avalanche photodiode), 112, 232
- Arabidopsis thaliana*. *See* Plants, live cell imaging of
- Articular cartilage, imaging tissue using AFM, 187–189, 188f
- AsRed2 (fluorescent protein), 12
- Assembly buffer (recipe), 600
- Atomic force microscopy (AFM), 183–301
advantages of, 183
for mechanical testing of biological samples, 186, 186f
microscope setup, 184–185, 184f
operating principles, 183–184
optical microscopy combined with, 184–185, 184f
perfusion of sample, 185
probes, 185
protocols
 imaging articular cartilage tissue, 187–189, 188f
 imaging collagen II, 194–197, 196f, 197f
 imaging fibroblast cells, 190–193, 190f, 191f
 microsphere tip preparation, 198–200, 199f
 temperature control, 185
ATP depletion, 630
ATV solution (recipe), 200–201
AutoAligner (software), 73t
Autofluorescence
 noise, 634
 in thick *Drosophila* specimens, 401
 in yeast, 343
Autofocus
 image-based, 288
 reflection-based, 288
AutoQuant (software), 702
Avalanche photodiode (APD), 112, 232
Avertin, 425
AxioVision (software), 289
Azami Green (fluorescent protein), 9t, 10
Azides, 528–529
Azurite (fluorescent protein), 7, 9t
- ## B
- Bacterial artificial chromosome (BAC)
 vectors, 542–543, 546, 552–555, 614
Bandpass filter, 325, 340, 340f, 349
Beer–Lambert law, 702, 706
Benchmarking, simulation-based, 279
Berkeley Madonna (software), 73t
BFP. *See* Blue fluorescent protein (BFP)
- Biarsenicals, labeling with
 fluorescent photoconversion of 1,2-diaminobenzidine tetrachloride (DAB), 465, 467–468, 468f, 469f, 472–474
live cell imaging for correlative microscopy, 465–467
 acquisition system design, 467
 cell growth imaging medium, 466–467
 chambers for live cell imaging, 465–466
 preparation of labeled cells, 465–467
 protocols
 fluorescence photoconversion of biarsenical-labeled cells for correlated EM, 472–474
 labeling tetracysteine-tagged proteins with biarsenical dyes, 470–471
 tetracysteine-tagged proteins, generating, 463–464
 transfection strategies, 464
Bimolecular fluorescence complementation (BiFC) assay
 for plant protein–protein interactions, 375–379
 split fluorescent proteins and, 29
 use of fluorescent protein fusions in, 35–36
Bind-silane working solution (recipe), 51
Binning, camera, 59–60, 60f, 65, 341
Bioconductor (software), 313
Bio-Formats, 286, 294
Biomechanical models, relating live cells to, 642
Bit depth, 285
 CCD camera, 59, 285
Blue fluorescent protein (BFP), 7, 9, 9t
Bodipy ceramide, 631
Boveri, Theodor, 351
Brefeldin A, 629
Brenner, Sydney, 352
Bright-field microscopy. *See also specific applications*
 magnetic twisting cytometry, 262
 passive microrheology, 265
 total internal reflection fluorescence (TIRF) microscopy, 683
Brightness, in live cell imaging, 337–342
 camera setup, 341–342
 choosing an objective, 338–339
 dichroic mirrors, 339, 340
 filters, 339–340, 339f, 340f
Brownian motion, 264
BS-C-1 cells, 572–573, 573t, 574f
Bubulya, Paula, 37
Bütschli, Otto, 351

722 ■ INDEX

- C**
- Caenorhabditis elegans*
description of, 351
GFPase in, 3
transformation-rescue experiments in, 353
- Caenorhabditis elegans*, live imaging of,
351–366
advantages to using, 351
data collection, 354–356
digital imaging, 356
fluorescent Fire vectors, 354–355
multiple focal-plane time-lapse
recording systems, 356
photographic records, 355
video microscopy, 355–356
examples, 356–358
analysis of individual larvae or adults
using confocal microscopy and
three-dimensional
reconstructions of vulval rings,
357–358
first divisions in early embryos and
chromatin dynamics in lamin
mutants, 356–357, 357f
simultaneous Nomarski and GFP
imaging of elongating
epidermal cells in embryos,
357, 358f
history of, 351–353
preparation of samples for, 353
protocols, 359–366
mounting of early embryos, 359
mounting of late-stage embryos,
larvae, or adults and slowing
their movement, 360–361
preparation and use of agarose pads
for microinjection, 364
preparation and use of agar pads for
live microscopy, 362–363
preparation and use of poly-L-lysine
coverslips for observation of
embryos, 365–366
recommendations for observing, 353–354
troubleshooting guide, 352t
- Caged fluorophores, 698
- Calcium- and magnesium-free phosphate-
buffered saline (recipe), 562
- Calcium biosensors, 27–28, 28f
- CAM (chick chorioallantoic membrane),
479, 501
- Cameleon (biosensor), 27
- Camera
CCD (*see* Charge-coupled device (CCD)
camera)
selection for total internal reflection
fluorescence (TIRF)
microscopy, 666
- Carlton, Peter, 204
- Cartilage
collagen II imaging using AFM, 194–197,
196f, 197f
imaging articular using AFM, 187–189,
188f
- Cauchy, 649
- CCD camera. *See* Charge-coupled device
(CCD) camera
- CCD chip, 54–56, 61–63, 64, 341, 341f
- Cell cycle, four-dimensional imaging of
plant cells during, 380–385
- CellProfiler (software), 313
- Cell segmentation, image analysis and,
243–245
deformable models and, 245
edge-based, 244
region-based, 244–245
threshold-based, 243–244, 244f
- Cell-Tak, 701
- Cell tracking, quantitative image analysis and
deformable models, 248–249
deterministic two-step approaches, 248
mitosis handling, 249–250, 249f, 250f
probabilistic approaches, 249
- Centromeres, tracking through mitosis, 384f
- Cerulean (fluorescent protein), 9–10
- CFP. *See* Cyan fluorescent protein (CFP)
- CFPAC-1 cells, 573, 573t
- Chalfie, Martin, 353
- Chambers for live cell imaging
correlative microscopy, 465–466
intravital microscopy in the mouse
dorsal skin chamber preparation in
mice, 490
mammary fat pad chamber
preparation in mice, 493
rabbit ear chambers, 488–489
mechanical stress, 643–649
membrane systems and membrane
traffic, 625–626
Rose chamber, 576–577, 581, 581f, 613,
689
total internal reflection fluorescence
(TIRF) microscopy, 689
in vivo imaging of mammalian cells,
319–320
dish-based chambers, 320
microchambers in slide format, 320
- Charge-coupled device (CCD) camera,
53–66
in atomic force microscope-light
microscope setup (AFM-LM),
184, 184f
binning, 59–60, 60f, 65, 341
bit depth, 59, 285
camera setup, 341–342
CCD chip, 54–56, 61–63, 64
architecture, 341, 341f
cooling, 323
Drosophila, live cell imaging in, 399
dynamic range, 59
electron bombardment CCD (EBCCD),
61–62
electron-multiplying charge-coupled
device (EMCCD), 62–63, 62f,
121, 133–135, 323, 399, 544,
679, 683
exposure time, 64
fluorescent protein use, 22
FRAP experiments and, 70–71
full well capacity, 59
how they work, 54–56, 55f
image acquisition, tips for, 63–65
binning use, 65
cool camera, 64
exposure time adjustment, 64, 64f
gain, setting, 65
grayscale values, monitoring, 63–64
offset, setting, 65
region of interest, choosing, 64
testing parameters, 65
image quality, 53–54, 54f
intensified (ICCD), 61, 420, 431
in magnetic twisting cytometry, 262
noise, 58–59, 62–63, 342
OMX, 204, 207, 209
photodiode/pixel size, 57–58
quantum efficiency, 57, 57f
readout, 56
resolution, 54, 57–58
RNA visualization and quantification,
702, 709
signal-to-noise ratio, 53–54, 64–65
subarray, 60–61
technical data sheet, 55f, 56
total internal reflection fluorescence and
spinning-disk confocal (TIRF/
SDC) microscope system,
121–122, 129, 130, 133–135
total internal reflection fluorescence
(TIRF) microscopy, 679, 683
- Chemical fluorophores, 69
- Chick chorioallantoic membrane (CAM),
479, 501
- Chromatic aberration
in confocal microscopy, 165, 176, 176f
description, 148, 176
imaging thick *Drosophila* specimens and,
400
- Chromatin dynamics, of *Caenorhabditis
elegans*, 356–357, 357f
- Chromosome tagging, 541–562
applications of, 541–542
lac operator direct repeats
cell lines containing, establishment of,
546–547
detection limits for, 543–545, 544f
recombinant DNA cloning of, 542–543
strategies for creating engineered
chromosome regions,
545–546, 545f
subcloning stable transformants,
547–548
overview of techniques for, 542
protocols
calcium phosphate transformation,
557
flow cytometry selection of stable
transformants with high-copy-
number chromosomal
insertions of DHFR transgene,
560
preparation of vector DNA, 550–551
purification and sterilization of
vector DNA, 556
subcloning using filter paper or
micropipette tips, 558–559
transposition of Tn5 transposon with
256mer *lac* operator repeat
and kan/neo selectable marker
into BAC DNA, 552–555
in vivo microscopy, 548–549
- Chronic window preparations, 476, 476f,
477t, 478
- Citrine (fluorescent protein), 9t, 11

- Classification, in quantitative image analysis, 240, 240f, 252–253
- Click chemistry, 529–530, 529f
- CLIP-170, 611, 614
- CLIP tag, 668, 670
- Clock-induced charge noise, 62–63
- CLSM. *See* Confocal laser-scanning microscopy (CLSM)
- C-MOS (complementary metal-oxide semiconductor) camera, 238
- Colcemid, 578
- Colchicine, 629–630
- Collagen dynamics, 484, 485f, 486
- Collagen II, imaging using AFM, 194–197, 196f, 197f
- Colonies, picking
with micropipette tip, 559
trypsin method for, 558–559
- Column buffer (recipe), 600
- Column buffer for inclusion bodies (recipe), 601
- Competent cells, preparation of *Agrobacterium tumefaciens*, 376
- Complementary metal-oxide semiconductor (C-MOS) camera, 238
- Computational image analysis
acquisition of optimized fluorescent images, 276–279, 277f
observation length, 278–279
sampling, 277–278, 278f
signal-to-noise ratio, 278
case study, 272–276
data-based diagnostics, 280, 280f
particle tracking, 272–276
motion modeling, 276
particle detection, 272, 273–274, 273f
trajectory construction, 272, 273f, 274–276, 275f
performance triangle of experimental setup, 276, 277f
simulation-based benchmarking, 279
why to use, 271–272
completeness, 272
consistency, 272
efficiency, 271–272
- COMSOL (software), 73t
- Confocal fluorescence microscopy
dynamic range, 225
illumination efficiency, 222
imaging speed, 225
lateral and axial extents of point-spread function, 223–224
light sheet-based fluorescence microscopy (LSFM)
compared, 215
lipid imaging in living cells, 526–527, 526f
photobleaching, 222–223
- Confocal laser-scanning microscopy (CLSM)
detector noise, 323
in FRAP experiments (*see* Fluorescence recovery after photobleaching (FRAP))
illumination and detection in, 328f
for membrane system and traffic imaging, 623, 625, 627–628, 633–637
photobleaching, 636–637
time-lapse experiment protocol, 633–635
tubulin and microtubule-associated proteins (MAPs), 614
- Confocal microscopy. *See also* Confocal fluorescence microscopy; Confocal laser-scanning microscopy (CLSM)
axial resolution, 169f
deconvolution of images, 163–165, 166f
environmental chamber for microscope, 161, 162f
features, 395t
fluorescent labels, 158–159
guidelines for generation of reliable images, 166–167
imaging modes, 157–158
instruments, 154–157
array scanning, 154f, 157, 168
beam scanning, 155–156
disk scanning, 154f, 156, 168, 178
multiple-pinhole, 156–157, 169f
point scanning, 395t, 678, 678t
slit scanning, 154f, 156, 395t
specimen scanning, 154–155
spinning-disk, 168, 169f, 178, 395t, 613, 678, 678t
spot scanning, 154, 154f, 168, 169f, 177–178
tandem scanning, 156–157
lasers, 158–159, 159t
limitations, 167–168
lipid imaging in living cells, 526–527, 526f
multiphoton microscopy compared to, 442–443, 443f
multiple labels, simultaneous imaging of, 159–160
optical principles, 151–154, 153f, 154f
patterned noise artifacts, 163, 164f
photobleaching and phototoxicity, 161–163, 162f
practical aspects of, 166
signal-to-noise ratio, 163, 164f, 165, 167, 177–179, 178f
specimen preparation, 160–161
thick specimen imaging, 151–172
total internal reflection fluorescence and spinning-disk confocal (TIRF/SDC) microscope system, 119–138
total internal reflection fluorescence (TIRF) microscopy compared, 678, 678t
troubleshooting, 168–172
tubulin and microtubule-associated proteins (MAPs) imaging, 613–614
wide-field microscopy compared, 152f, 153f, 169f, 178f
- Contrast enhancement, nonlinear, 290
- Contrast reversals, 143–144, 143f, 144f, 163, 163f
- Contrast-transfer function (CTF), 141–145, 143f
- Convolution, 144
discrete, 241
- Corneal pocket assay in rabbits, 477t, 479, 479f, 500
- Correlative microscopy, live cell imaging for, 463–474
acquisition system design, 467
microscope configurations, 467
signal detection, 467
cell growth imaging medium, 466–467
chambers for live cell imaging, 465–466
fluorescent photoconversion of 1,2-diaminobenzidine tetrachloride (DAB), 465, 467–468, 468f, 469f, 472–474
preparation of labeled cells, 465–467
protocols
fluorescence photoconversion of biarsenical-labeled cells for correlated EM, 472–474
labeling tetracysteine-tagged proteins with biarsenical dyes, 470–471
- Cranial window preparation in mice and rats, 476f, 477t, 491–492
- Critical angle, 676, 676f
- CTF (contrast-transfer function), 141–145, 143f
- Cyan fluorescent protein (CFP), 9–10, 9t
for imaging gene expression in living cells, 566–568, 569f
multiphoton imaging of tumors in vivo, 445, 445f, 448–449, 450f
tetracysteine-tags and biarsenicals, use of, 467
vimentin, 587, 587f
- Cycloheximide, 630
- CyGEL, 322
- Cytochalasin B, 630
- Cytomegalovirus promoter, 36, 612, 700
- Cytoskeleton
dynamics, imaging, 691, 693f
methods for expressing and analyzing GFP-tubulin and GFP-microtubule-associated proteins, 605–617
- Cytotoxicity, photobleaching-induced, 80–81
- ## D
- DAB (1,2-diaminobenzidine tetrachloride), fluorescent photoconversion of, 465, 467–468, 468f, 469f, 472–474
- DAG (diacylglycerol), 523, 530
- Data acquisition
acquiring a digital imaging, 287
autofocus, 288
computer control of imaging devices and peripherals, 288–289
maximizing information content, 287–288
software tools, 289
- Data mining, 311–312
- Deblurring, 290
- Deconvolution, 140–150
of confocal images, 163–165, 166f
constrained iterative, 145–147, 146f, 147f
deblurring techniques, 290
image preprocessing, 242–243
limitations of, 149–150
optical principles and, 140–144
restoration techniques, 290

724 ■ INDEX

- Deconvolution (*continued*)
 in RNA quantification, 702
 tips for reliable image generation, 148
 of wide-field microscope images,
 144–148, 147f
- Delaunay triangulation function, 652
- Dendra2 (fluorescent protein), 16f, 17, 453,
 454, 454f
- Denoising, in image preprocessing, 241–242,
 243f
 linear filters, 241–242
 nonlinear filters, 242, 243f
- Detector noise, 323
- Detergent buffer (recipe), 601
- DFCS culture medium (recipe), 201
- Diacylglycerol (DAG), 523, 530
- Dialysis buffer (recipe), 602
- Dialysis buffer for inclusion bodies (recipe),
 601
- 1,2-diaminobenzidine tetrachloride (DAB),
 fluorescent photoconversion
 of, 465, 467–468, 468f, 469f,
 472–474
- Dichroic mirrors, 339, 340, 420, 664–665
- Differential interference contrast (DIC), 149
 in passive microrheology, 265
 total internal reflection fluorescence and
 spinning-disk confocal (TIRF/
 SDC) microscope system, 119,
 125
- Diffraction limit, 334
- Diffusion, in photoperturbation
 experiments, 86–91
- Diffusion time, fluorescence correlation
 spectroscopy (FCS) and, 230,
 236–237
- Digital images
 Bio-Formats, 286
 bit depth, 285
 description of, 284
 file format tools, 286
 metadata, 285
 monochrome vs. color, 285
 multidimensional five-dimensional
 image, 284
 proprietary file formats, 285–286
 software tools for, 284–287
 standardized file formats, 286–287
- Digital scanned laser light sheet fluorescence
 microscopy (DSLM), 215–227
 advanced implementations of, 227, 227f
 comparison with other microscopy
 forms, 221–226
 cost efficiency, 226
 dynamic range, 225–226
 illumination efficiency, 221–222
 illumination pattern, 224
 imaging speed, 224–225
 lateral and axial extents of point-
 spread function, 223–224
 performance, 226f
 photobleaching, 222–223
 components, 216, 218–220, 218–221, 218f
 computer/software, 220
 detection system, 218–219, 221
 illumination system, 216, 218,
 220–221
 technical blueprint, 218–219
 features, 395t
 overview, 215–216
 sample images, 217f
- Dihydrofolate reductase gene, 545, 545f, 547,
 560, 565
- Diiodomethane, 677
- Diode-pumped solid-state (DPSS) lasers, 681
- Disassembly buffer (recipe), 602
- Discosoma striata*, 12
- Displacement index, 650
- DMF (recipe), 115
- DNA
 preparation of large quantities of vector
 DNA, 550–551
 purification and sterilization of vector
 DNA by ethanol precipitation,
 556
- Doppler OFDI (optical frequency domain
 imaging), 482, 482f, 487
- Dorsal skin chamber preparation in mice,
 476, 476f, 477t, 490
- DPSS (diode-pumped solid-state) lasers, 681
- Dronpa (fluorescent protein), 17, 70
- Drosophila*, live cell imaging in, 387–415
Drosophila as a model organism, 338t,
 387
 examples of, in different tissues, 389t
 as experimental approach, 401–402
 fluorescence microscopy techniques, new
 and emerging, 402–404
 fluorescent reagents, 391–394
 external application of dyes, 391–392
 fluorescent proteins, 393–394
 microinjection, 392–393, 392f
 preparation of material, 388–391
 optimal conditions for culturing
 tissues, 390t
 tissues amenable to time-lapse
 imaging, 388
 tissue viability, maintaining, 388,
 390–391, 391f
- protocols
 collection and mounting of embryos,
 407–409, 407f
 isolation of egg chambers, 405–406,
 405f
 larval fillet preparation and imaging
 neurons, 413–415, 414f
 macrophage preparation and
 screening, 410–412, 410f, 411f
 selection imaging equipment and
 methodology, 394–399
 contrast-enhancing bright-field
 methods, 397
 detectors, 399
 fluorescence-imaging system
 selection, 397–398, 397f
 imaging techniques, 395t
 microscope selection, 394, 396f
 microscope system evaluation, 394
 objective selection, 398, 399t
 optimizing excitation and emission,
 398
 thick specimens, problems with imaging,
 399–401
- DSLM. *See* Digital scanned laser light sheet
 fluorescence microscopy
 (DSLM)
- DsRed (fluorescent protein), 11, 12, 612
- Dulbecco's PBS (recipe), 536
- Dyes, organelle-specific, 631
- Dynamic range, CCD camera, 59, 225–226
- Dynein
 molecule movement, kymographs of,
 666–667, 666f
 motility assay (protocol), 673–674
- E
- EBCCD (electron-bombardment CCD),
 61–62
- EBFP. *See* Enhanced blue fluorescent protein
 (EBFP)
- EB1-GFP, 611
- ECFP. *See* Enhanced cyan fluorescent protein
 (ECFP)
- ECM (extracellular matrix), multiphoton
 imaging and, 442–443
- ECM coating solution (recipe), 51
- EGF (epidermal growth factor), 95, 458–459
- EGFP. *See* Enhanced green fluorescent
 protein (EGFP)
- EGF receptor (EGFR) phosphorylation,
 97–101, 99f, 101f, 103
- Egg chambers, isolation of *Drosophila*,
 405–406, 405f
- Egg salts solution (recipe), 366
- Elastic modulus, 258, 258f, 259, 261f, 266
- Electron-bombardment cooled charge-
 coupled device (EBCCD),
 61–62
- Electron microscopy, correlated live cell light
 microscopy with, 463–474
- Electron-multiplying cooled charge-coupled
 device (EMCCD), 62–63, 62f,
 121, 133–135, 323, 399, 544,
 679, 683
- Electroporation, for transfection of
 mammalian cells, 36, 37,
 38–39
- Emerald (fluorescent protein), 9t, 10, 16
- Endocytosis, imaging, 691, 694f
- Endogenous tracers, as probes for passive
 microrheology, 265
- Endosperm, 571
- Enhanced blue fluorescent protein (EBFP),
 7, 9t
- Enhanced cyan fluorescent protein (ECFP),
 4f, 6, 9t, 10, 372
- Enhanced green fluorescent protein (EGFP),
 4f, 5, 9t, 10, 69–70, 71, 372
lac operator-tagged, 543, 544, 546, 547
 tubulin tagging, 611–612
- Enhanced yellow fluorescent protein (EYFP),
 4f, 6, 9t, 11, 372
- Entacmaea quadricolor* (sea anemone), 12
- Environmental control
 devices, 345–346
 in vivo imaging of mammalian cells, 319
- Eos (fluorescent protein), 16f, 17
- Epidermal growth factor (EGF), 95, 458–459
- Epifluorescence microscopy
 for intravital microscopy, 480, 480f
 optical elements of, 339–340, 339f
 total internal reflection fluorescence
 (TIRF) microscopy, 684, 692

- ER tracker, 631
 Ethyl carbamate, 425
 Excess noise factor, 63
 Exocytosis, imaging, 691–692
 Extracellular matrix (ECM), multiphoton imaging and, 442–443
 Extraction buffer (recipe), 600
 EYFP. *See* Enhanced yellow fluorescent protein (EYFP)
- F**
- FIAsH-EDT2, 41, 632
 FCCS. *See* Fluorescence cross-correlation spectroscopy (FCCS)
 FCS. *See* Fluorescence correlation spectroscopy (FCS)
 FIAsH (biarsenical reagent), 464, 467–468, 470
 Fibroblasts, imaging using AFM, 190–193, 190f, 191f
 FIDA (fluorescence intensity distribution analysis), 231
 File formats, for digital images, 285–287
 File system, storing data on, 293
 Filters
 acousto-optical tunable filters (AOTFs), 71, 75, 663, 681
 epifluorescence microscope, 339–340, 339f, 340f
 bandpass, 340, 340f, 349
 high-pass, 340, 340f
 neutral density, 340
 short-pass, 340, 340f
 fluorescein isothiocyanate (FITC) filter sets, 10, 11
 identifying optimal, 610
 for image denoising,
 linear filters, 241–242
 nonlinear filters, 242, 243f
 Kalman, 251–252
 total internal reflection fluorescence (TIRF) microscopy, 664–665
- Fire, Andrew, 353
 Fire vectors, 354–355, 354t
 FISH (fluorescent in situ hybridization), 697, 702, 706–710
 FITC, caged, 402
 FLIM. *See* Fluorescence lifetime imaging microscopy (FLIM)
 FLIP. *See* Fluorescence loss in photobleaching (FLIP)
 Flow cytometry, selection of stable transformants with high-copy-number chromosomal insertions of DHFR transgene, 560
 Fluorescein isothiocyanate (FITC) filter sets, 10, 11
 Fluorescence correlation spectroscopy (FCS), 101–102, 229–238
 autocorrelation curve shift, 236–238
 diffusion time, 230
 as function of viscosity, 236–237
 FRAP, discrepancy of results with, 91–92
 parameters and properties, 230–231, 231f
 count rate per molecule, 231
 diffusion time, 230
 number of molecules, 230
 setup and measurement protocol, 232–235
 determination of structure parameter, 233
 initial adjustment, 232
 initial measurement, 232
 laser power adjustment, 233–234, 233f
 laser power for in vivo measurements, 234
 laser power plot vs. count per molecule, 234
 materials, 232
 troubleshooting, 234
 total internal reflection (TIR-FCS), 236–238, 684
 Fluorescence cross-correlation spectroscopy (FCCS), 96, 96f, 101–102
 measuring protein interaction by, 114–115
 Fluorescence-decay profile, 100–101
 Fluorescence intensity distribution analysis (FIDA), 231
 Fluorescence lifetime, 100–101, 101f
 Fluorescence lifetime imaging microscopy (FLIM), 100–101, 101f, 112–113, 402, 451, 683
 Fluorescence loss in photobleaching (FLIP), 68, 68f, 77, 78, 83, 587, 589
 Fluorescence microscopy
 confocal
 dynamic range, 225
 illumination efficiency, 222
 imaging speed, 225
 lateral and axial extents of point-spread function, 223–224
 light sheet-based fluorescence microscopy (LSFM)
 compared, 215
 lipid imaging in living cells, 526–527, 526f
 photobleaching, 222–223
 lipid imaging in living cells, 526–527
 confocal microscopy, 526–527, 526f
 total internal reflective fluorescence (TIRF) microscopy, 527, 527f
 wide-field microscopy, 526
 resolution, 57–58
 Fluorescence photoactivated localization microscopy (F-PALM), 404
 Fluorescence photoconversion, 463, 465, 467–468, 468f, 469f, 472–474
 Fluorescence ratio imaging microscopy (FRIM), 514
 Fluorescence recovery after photobleaching (FRAP), 67–92, 238, 402
 analysis of time-lapse acquisitions, 81–83
 background subtraction, 82, 82f
 corrections, 82–83, 82f
 image alignment, 81–82
 normalization, 82f, 83
 photobleaching, 82, 82f
 steps in image analysis, 82f
 artifacts
 cell movement, 81
 cytotoxicity, 80–81
 focus drift, 81
 laser intensity fluctuations, 80
 reversible photobleaching, 79–80
 bleaching-induced cellular damage, 80–81
 calibrating 3D shape of photoperturbed region, 78
 controls, 79
 experimental technique, 74–78
 deciding when to stop, 78
 image acquisition parameters, 74–75, 77
 photoperturbation, 77–78
 prebleached image acquisition, 77
 fluorescent probes, 69–70
 chemical fluorophores, 69
 dark states of, 76f, 79–80
 photoactivatable, 70
 for photobleaching, 69–70
 photoconvertible, 70
 future of, 91–92
 GFP-lamin, 587, 589
 image acquisition parameters
 detector gain and offset, 75, 77
 laser power and transmission, 75
 pinhole settings, 74–75
 scan speed/scan average/acquisition frequency, 75, 76f
 scan zoom/scan field, 75
 intravital microscopy in mice, 487
 inverse (iFRAP), 68, 627–628, 627f
 microscope setup, 70–73
 laser fluctuation, controlling, 71
 laser selection, 71
 microscope objectives, 71–73, 72f
 photoperturbation mode, 71
 software for microscope operation, 73
 modeling redistribution kinetics, 83–91
 averaging parameters from different cells, 91
 diffusion and reaction limited redistribution, 91
 diffusion-limited redistribution, 86–87, 87f, 89, 90f
 interaction-limited redistribution, 86–87, 87f, 89
 qualitative analysis, 83, 84f
 quantitative analysis, 83–84
 space independent variables, defining, 85–86
 spatial diffusion-reaction modeling, 85, 85f
 two-dimensional vs. three-dimensional modeling, 86, 87f
 reversibility of bleaching, 79–80
 software for data analysis, 73, 73t
 techniques commonly used, 67–68, 68f
 Fluorescence resonance energy transfer (FRET), 402
 acceptor photobleaching, 98–99, 99f, 108–110
 biosensors, 26–29
 description, 97
 dimerization of fluorescent protein fusions, 7
 fluorophore pair, choosing, 97, 98f
 lipid imaging in living cells, 523
 protocols
 acceptor photobleaching, 108–110
 antibody labeling with fluorescent dyes, 103–105
 cell preparation for FRET, 106–107

726 ■ INDEX

- Fluorescence resonance energy transfer
(*continued*)
measurement by confocal time-correlated single-photon counting fluorescence lifetime imaging, 112–113
measurement by sensitized emission, 111
quantification
by donor quenching, 97–99, 99f
by fluorescence lifetime imaging, 100–101, 101f
by sensitized emission of the acceptor, 99–100, 111
tetracysteine tags and biarsenicals, use of, 467
- Fluorescent analog cytochemistry, 605–606
- Fluorescent dye, antibody labeling with, 103–105
- Fluorescent Fire vectors, 354–355, 354t
- Fluorescent images, acquisition of
optimized, 276–279, 277f
observation length, 278–279
sampling, 277–278, 278f
signal-to-noise ratio, 278
- Fluorescent in situ hybridization (FISH), 697, 702, 706–710
- Fluorescent photoconversion. *See* Fluorescence photoconversion
- Fluorescent protein fusions (FPFs)
constructing, 35–36
expressing, 36–37
functionality of protein, 40–41
localization of protein, 40
transfection of mammalian cells (protocol), 38–41
folding of, 36
for live cell imaging of plants, 372–374
cloning strategies, 372–373
transferring vectors into
Agrobacterium, 373
transgenic plants expressing, generation of, 373
validating by rapid, transient expression, 373
for in vivo imaging of mammalian cells, 318–319
- Fluorescent proteins (FPs)
applications, 18–29
biosensors, 26–29, 27f
common uses in living cells, 18
digital imaging tips, 21–22
multicolor imaging, 22–25
practical aspects of use, 18–21, 19f, 20f
specialized, 25–29
biosensors
bimolecular fluorescence complementation (BiFC) assay, 29
calcium, 27–28, 28f
phosphorylation, 28
protease-cleavage assay, 28
strategies for, 26–27, 27f, 29
color variants, 7–13
blue, 7, 9, 9t
cyan, 9–10, 9t
green, 9t, 10 (*see also* Green fluorescent protein)
orange, 9t, 11–12
red, 9t, 12–13
yellow, 9t, 11
dark states of, 76f, 79–80
expression schemes for, 689
filter sets, identifying optimal, 610
future directions, 29
for live cell imaging of *Drosophila*, 393–394
for live cell imaging of plants, 371–372
for live imaging by subcellular localization, 355t
localization of FP fusions, 7, 8f, 20–21, 21f
long Stokes shift, 13
monomeric, 6–7
multicolor imaging, 22–25
with spectral detection, 24–25, 24f, 25f
without spectral detection, 24–25, 24f, 25f
mutations for use in mammalian systems, 6
in OMX microscopy, 207, 209
optical-highlighter, 13–14, 14t, 15f
photoactivatable, 14, 16, 70
for photobleaching, 69–70
photoconvertible, 16–17, 70
photoswitchable, 17–18
structure, 4–5, 4f
in vivo imaging of mammalian cells, 317–318
- Fluorescent speckle microscopy (FSM), 119, 120, 292
- Fluorophores
caged, 698
chemical, 69
lipid imaging in living cells, 529–530
multiphoton imaging of tumors in vivo, 448–451, 449f, 450f
in vivo imaging of mammalian cells, 318
- Focus drift, 635
- Force-curve measurements, 186, 186f
- Force mapping, 186, 187, 188f, 191f
- Force-volume map, 191f
- Förster distance, 98f
- Four-dimensional microscopy
imaging of plant cells during cell cycle (protocol), 380–385
multiple focal-plane time-lapse recording systems for *Caenorhabditis elegans*, 356
- F-PALM (fluorescence photoactivated localization microscopy), 404
- FPFs. *See* Fluorescent protein fusions (FPFs)
- FPS. *See* Fluorescent proteins (FPs)
- FRAP. *See* Fluorescence recovery after photobleaching (FRAP)
- FRAP Analyser (software), 73t
- FRAP Analysis (software), 73t
- Free radical scavengers, 466–467
- FRET. *See* Fluorescence resonance energy transfer (FRET)
- FRIM (fluorescence ratio imaging microscopy), 514
- Fruit fly. *See* *Drosophila*, live cell imaging in
- FSM (fluorescent speckle microscopy), 119, 120, 292
- FuGENE 6, 192
- Full well capacity, CCD camera, 59
- Full width at half-maximum (FWHM), 175
- Fusion proteins. *See* Fluorescent protein fusions (FPFs)
- ## G
- Gain, setting CCD camera, 65
- Gene expression, imaging in living cells, 565–569, 569f
schematic of gene-expression plasmid p3216PECMS2 β , 567f
- Genetic tags, self-labeling, 668
- Germination plates (recipe), 385
- GFP. *See* Green fluorescent protein (GFP)
- Global-nearest-neighbor (GNN) algorithm, trajectory construction and, 274, 275
- Glycosyl phosphatidylinositol-GFP (GPI-GFP), 627, 627f
- Goldberg, Ilya, 294
- Golgi complex, imaging of, 623, 624f, 625f, 627–628, 627f, 629f, 631, 632f
- Green fluorescent protein (GFP). *See also* fluorescent protein fusions (FPFs); Fluorescent proteins (FPs)
actin tagged with, 190–193, 190f
advantages over fluorescent analog chemistry, 606
color variants, 7–13
in cytoskeleton analysis, 605–617
disadvantages of system, 606
discovery of, 3
features of *Aequorea victoria*, 4–6
filters for, 340
fusion proteins
construction, 35–36
functionality, determination of, 40–41
localization, determination of, 40
for imaging gene expression in living cells, 565
intermediate filament proteins, GFP-tagged, 584–590, 586f–589f
characterizing, 585
constructing and expressing, 585
keratin, 586–587, 587f
lamins, 587–590, 588f, 589f
peripherin, 586f
type-I and type II IFs, 586–587
type-III IFs, 585–586
type-V IFs, 587–590, 588f, 589f
vimentin, 584–586, 585f, 586f, 587f, 599–600
for membrane system and traffic imaging, 623, 625–628, 631–632, 632f
microtubule-associated proteins (MAPs), GFP-tagged
construction of, 611–612
examples of microtubule-binding protein fusion to fluorescent proteins, 608t–609t
microscopy, 613–614
overexpression, issues associated with, 614
overview of, 610–611
transfection of, 612–613
MS2-GFP system, 698–710

- multiphoton imaging of tumors in vivo, 444–445, 445f, 447–449, 450f, 451, 453, 457
 mutations that improve use in mammalian systems, 6
 photoactivatable (PA-GFP), 14, 16, 70, 615, 628
 structure, 4–5, 4f
 tetracysteine tags and biarsenicals, use of, 467
 tubulin, GFP-tagged
 construction of, 611–612
 examples of tubulin fusion to fluorescent proteins, 607t
 history of, 610
 microscopy, 613–614
 overview, 610
 permanent cell lines for expression of, 613, 615–617
 transfection of, 612–613
 Ground-state depletion, 159
 Gustafsson, Mats, 203–204
- H**
- Halocarbon oil, 390–391, 391f, 392, 405–406, 407, 409
 HaloTag, 668, 670
 Haralick features, 310
 Haziness index, 179
 HcRed1 (fluorescent protein), 12, 372
 Hell, Stefan, 403
 Helmholtz coils, 261–262
 HEPES buffer (recipe), 537
 Heptane glue, 407, 408
 Heterodyning, 262
 High-content screening microscopy, 297–314
 assay development, 297–300, 298f, 299f
 data handling and processing, 306–313
 experimental setup, 304–306
 microscopy system requirements, 302–304
 sample preparation, 300–302
 Highly ordered pyrolytic graphite (HOPG), as substrate for AFM, 194, 195–196
 Histone acetyltransferase, 566
 Histone H3 variant fusions, 380–385
 Hit detection, 311
 Homogenization buffer (recipe), 601
 Homogenization buffer for inclusion bodies (recipe), 601
 Hooke's law, 183
 HOPG (highly ordered pyrolytic graphite), as substrate for AFM, 194, 195–196
 Horvitz, H. Robert, 352
 Huygens Professional (software), 702
- I**
- I-CCD (intensified CCD), 61, 420, 431
 IDL (Interface Definition Language), 292
 IFRAP (inverse fluorescence recovery after photobleaching), 68, 627–628, 627f
 IGOR Pro (software), 313
 Illumination efficiency
 digital scanned laser light sheet
 fluorescence microscopy (DSLMS), 221–222
 Illumination noise, 323
 ILOV, 372
 Image acquisition
 fluorescence recovery after photobleaching (FRAP), 74–75, 77
 fluorescent images, 276–279, 277f
 mammalian cells, in vivo imaging of, 326–329
 acquisition system, choice of, 327–328, 328f
 photodamage, 326–327
 rate of acquisition, 329
 two-dimensional vs. three-dimensional images, 326
 variability in behavior between different cells, 327
 software tools for, 289
 Image analysis. *See also* Computational image analysis; Quantitative image analysis
 critical applications for, 292–293
 machine learning methods, 292
 object definition, 291
 object measurement, 291–292
 tools for, 292
 Image data management
 applications, 293–294
 file system, 293
 software tools, 293–294
 ImageJ (software), 73t, 286, 287, 291, 292, 356, 374, 457, 628
 Image preprocessing, 240, 240f, 241–243, 242f
 deconvolution, 242–243
 denoising, 241–242, 243f
 linear filters, 241–242
 nonlinear filters, 242, 243f
 Image processing
 deconvolution, 290
 fundamentals of, 290
 nonlinear contrast enhancement, 290
 platforms, 290–291
 software tools for, 290–291
 Image-Pro Plus (software), 289
 ImageReady CS2, 457
 Imaging buffer (recipe), 538
 Imaging chambers
 correlative microscopy, 465–466
 intravital microscopy in the mouse
 dorsal skin chamber preparation in mice, 490
 mammary fat pad chamber preparation in mice, 493
 rabbit ear chambers, 488–489
 mechanical stress, 643–649
 membrane systems and membrane traffic, 625–626
 Rose chamber, 576–577, 581, 581f, 613, 689
 total internal reflection fluorescence (TIRF) microscopy, 689
 in vivo imaging of mammalian cells, 319–320
 dish-based chambers, 320
 microchambers in slide format, 320
 Imaging medium (recipe), 638
 Immunoblot analysis, of fluorescent protein fusions, 40–41
 Immunofluorescence, for determination of protein fusion location, 40
 Impulse response of microscope, 334
 Incubator, air-curtain, 577
 Inducible promoter system, 612
 Information capacity, 336–337
 Information content, of acquired images, 287–288
 Interference reflection contrast microscopy (IRM), 157–158, 158f
 Intermediate filaments (IFs), imaging, 583–602
 GFP-tagged IF proteins, 584–590
 characterizing, 585, 586f
 constructing and expressing, 585
 keratin, 586–587, 587f
 lamins, 587–590, 588f, 589f
 peripherin, 586f
 type-I and type II IFs, 586–587
 type-III IFs, 585–586
 type-V IFs, 587–590, 588f, 589f
 vimentin, 584–586, 585f, 586f, 587f, 599–600
 mechanical stress analysis, 649–652, 650f
 choosing a length scale for subcellular analysis, 650–651
 computation of displacement index, 651–652
 microinjection of fluorochrome-labeled IF proteins, 584
 overview, 583
 protocols
 microinjection of X-rhodamine vimentin, 597–598
 purification of bacterially expressed vimentin, 593–594
 purification of bovine vimentin, 591–592
 transfection of cells with GFP-tagged vimentin, 599–600
 X-rhodamine labeling of vimentin, 595–596
 Internal ribosome entry site (IRES), 615
 Intravital microscopy in the mouse, 475–518
 future perspectives, 487
 intravital microscopy workstations, 480–482, 480f
 conventional single-photon microscopy, 480–481, 480f
 multiphoton laser-scanning microscope (MPLSM), 480f, 481
 optical frequency domain imaging (OFDI), 481–482, 482f
 protocols, 488–518
 CAM (chick chorioallantoic membrane), 501
 corneal pocket assay in rabbits, 500
 cranial window preparation in mice and rats, 491–492
 dorsal skin chamber preparation in mice, 490
 extravascular parameters: interstitial and microvascular pO₂ measurements, 515–516

728 ■ INDEX

- Intravital microscopy in the mouse
(*continued*)
 extravascular parameters: interstitial diffusion, convection, and binding, 517–518
 extravascular parameters: interstitial pH measurement, 514
 liver tumor preparation in mice, 498
 lung window preparation in mice, 495–496
 mammary fat pad chamber preparation in mice, 493
 mammary fat pad preparation in mice, 499
 mesentery preparation in mice and rats, 497
 mouse ear model, 504–505
 pancreatic tumor preparation in mice, 494
 rabbit ear chambers, 488–489
 tail lymphatics in mice, 502–503
 vascular parameters: angiogenesis and hemodynamics, 506–509, 506f
 vascular parameters: leukocyte-endothelial interactions, 512–513
 vascular parameters: vascular permeability, 510–511
 surgical procedures for tissue preparations, 476–480
 acute (exteriorized) preparations, 477t, 478, 478f
 chronic window preparations, 476, 476f, 477t, 478
 examples of preparations for tumor studies, 477t
 in situ preparations, 477t, 479–480, 479f
 tumor growth and regression, 482–486
 collagen dynamics using second harmonic generation, 484, 485f, 486
 extravascular parameters, 483, 483t
 gene expression, 484
 lymphangiography, 483–484, 484f, 486
 promoter activity via GFP imaging, 484, 485f
 vascular parameters, 483, 483t
 Inverse fluorescence recovery after photobleaching (IFRAP), 68, 627–628, 627f
 In vivo invasion assay, 455–456, 455f, 458–459
 IRES (internal ribosome entry site), 615
 IRM (interference reflection contrast microscopy), 157–158, 158f
 Isofluorane, 425, 447, 448, 453, 459
- J**
 JRed (fluorescent protein), 12
- K**
 Kaede (fluorescent protein), 16f, 17
 Kalman filter, 251–252
 Katushka (fluorescent protein), 13
 Keima (fluorescent protein), 13
 Keratin, GFP-tagged, 586–587, 587f
 Ketamine, 448
 KikGR (fluorescent protein), 16f, 17
 Kindling (fluorescent protein), 17–18
 Koehler wide-field epi-illuminator, 125–128
 Kymographs, 66f, 666–667
- L**
 LabVIEW, 289, 450
lac operator, 565–567, 567f
lac operator direct repeats
 cell lines containing, establishment of, 546–547
 detection limits for, 543–545, 544f
 preparation of vector DNA containing, 550–551
 purification and sterilization of vector DNA containing, 556
 recombinant DNA cloning of, 542–543
 strategies for creating engineered chromosome regions, 545–546, 545f
 subcloning stable transformants, 547–548
 transposition of Tn5 transposon with 256mer *lac* operator repeat and kan/neo selectable marker into BAC DNA, 552–555
 Lagrangian strain tensor, 652
 Lamins, GFP-tagged, 587–590, 588f, 589f
 LAP (linear assignment problem), 274, 275
 Laser light, activating photoactivatable proteins with, 638
 Lasers
 for confocal microscopy, 158–159, 159t
 for total internal reflection fluorescence (TIRF) microscopy, 680–681, 680f
 combining and attenuation, 681
 conventional lasers, 681
 diode-pumped solid-state (DPSS) lasers, 681
 single-mode fiber and, 681
 Laser-scanning confocal microscope (LSCM), 402, 403
 Latrunculin A, 630
 LB liquid medium (recipe), 561
 LB plates (recipe), 561
 Lens aberrations, 348f
 LIBSVM (software), 313
 Light microscopy. *See also specific applications*
 atomic force microscopy combination (AFM-LM), 184–185, 184f
 correlated with electron microscopy, 463–474
 Light sheet–based fluorescence microscopy (LSFM), 215–216, 216f
 Linear assignment problem (LAP), 274, 275
 Linear filters, 241–242
 Linear viscoelasticity, 259
 Lipid mix A (recipe), 537
 Lipid mix B (recipe), 538
 Lipids, imaging in living cells, 523–538
 direct labeling of lipids in cells, 528–530
 chemistry inside living cells, 528–529
 clickable synthetic lipids, 530
 click chemistry, 529, 529f
 fluorophores, 529–530, 529f
 lipid entry into cells, 530
 fluorescence microscopy, 526–527
 confocal microscopy, 526–527, 526f
 total internal reflective fluorescence (TIRF) microscopy, 527, 527f
 wide-field microscopy, 526
 lipid-binding domains as lipid detectors, 524–528
 construction of VFP-tagged lipid-binding domains, 524–525
 fluorescence microscopy, 526–527
 time-lapse experiments and quantification, 528
 protocols
 lipid labeling in fixed cells, 533–534, 534f
 lipid labeling in living cells, 535–538, 536f
 transfection of cells with DNA encoding a VFP-tagged lipid-binding domain, 531–532
 Lipofectamine 2000, 318, 531–532, 612
 Liver tumor preparation in mice, 477t, 478f, 498
 LLC-Pk1 cells, 572–574, 573t, 574f, 575f
 Localization, of fluorescent protein fusions, 40
 Local-nearest-neighbor (LNN) algorithm, trajectory construction and, 274, 275f
 Long-pass filter, 325
 LSCM (laser-scanning confocal microscope), 402, 403
 LSFM (light sheet–based fluorescence microscopy), 215–216, 216f
 Lung window preparation in mice, 476, 477t, 478, 495–496
 Luria–Bertani (LB) liquid medium (recipe), 384–385
 Lymphangiography, 483–484, 484f, 486, 503
 LysoTracker, 631
- M**
 Machine-learning approach, 307
 Macrophage preparation and screening, 410–412, 410f, 411f
 Magnetic beads, 260–261
 Magnetic pulling, 258f
 Magnetic tweezers, 259, 263
 Magnetic twisting cytometry (MTC), 258f, 260–264
 calibration, 262
 cell types, 262
 data analysis, 262–263
 experimental requirements for, 260–262
 imaging, 262
 limitations of, 263–264
 magnetic beads, 260–261
 magnetic-field source, 261–262
 protocol, 268–269
 schematics, 261f
 mAmetrine (fluorescent protein), 13
 Mammalian cells
 cytoskeleton dynamics and, 611–617
 mitosis studies in cultured cells, 571–582
 cell synchronization, 578
 characteristics of cultured cell lines, 573t
 culturing cells for study, 575–578, 579

- mitotic phase maintenance, 577–578
- mounting coverslips, 576–577, 580–582
 - protocols, 579–582
- growing cultured cells, 579
- mounting coverslips for imaging, 580–582
 - Rose chambers, 576–577, 581, 581f
 - temperature maintenance, 577
- transfection of, 38–41
- Mammalian cells, high-content screening, 297–314
 - assay development, 297–300, 298f, 299f
 - dimensions and stage-movement strategies, 299f
 - project workflow, 298f
- data handling and processing, 306–313
 - automatic quality control, 312
 - classification, 310–311
 - data mining, 311–312
 - feature extraction, 310
 - image-processing strategies to analyze time-lapse image data, 307, 308f
 - implementation and software packages, 312–313, 313t
 - segmentation, 309
 - time series and hit detection, 311
 - tracking, 309–310
- experimental setup, 304–306
 - environment, 305
 - spatial resolution, 305
 - temporal resolution, 304–305
- microscopy system requirements, 302–304
 - automation, 303
 - compatibility, 304
 - instruments, table of, 302t
 - stability, 303–304
- sample preparation, 300–302
- Mammalian cells, in vivo imaging of, 317–330
 - cell and media conditions, 321–322
 - free-radical scavengers, 321
 - osmolarity, 322
 - oxygen-depletion systems, 321
 - pH, 321
 - pH indicators, 321
 - cell engineering, 317–319
 - considerations regarding expressed fluorescent protein fusions, 318–319
 - fluorescent protein functionality, 317–318
 - labeling with small-molecule fluorophores, 318
 - transfection strategies, 318
 - evaluation of results, 329–330
 - establishing criteria for cell viability, 329
 - fixed cell time-point assays, 330
 - long-term time lapse, 329–330
 - image acquisition, 326–329
 - acquisition system, choice of, 327–328, 328f
 - photodamage, 326–327
 - rate of acquisition, 329
 - two-dimensional vs. three-dimensional images, 326
 - variability in behavior between different cells, 327
- microscope optics, 324–326
 - aberrations that reduce signal-to-noise ratio, 325–326
 - fluorescence filter sets, 325
 - objective-lens correction, 325
 - objective-lens magnification, 324–325
 - objective-lens numerical aperture, 324
- noise sources, 323–324
 - detector noise, 323
 - illumination noise, 323
 - Poisson or shot noise, 323–324
 - stray light/spurious photons, 323–324
- strategies for maintaining cell viability and health during imaging, 319–322
 - cell and media conditions, 321–322
 - environmental control, 319
 - examination of cells before and during the imaging experiment, 322
 - imaging chambers, 319–320
 - imaging nonadherent cells, 322
 - open vs. closed chambers, 319
 - temperature control, 320
- Mammary fat pad chamber preparation in mice, 493
- Mammary fat pad preparation in mice, 478f, 499
- Mammary-imaging window, 452–455, 452f
- MAP2, 610
- MAPK (mitogen-activated protein kinase) pathway, 95
- mApple (fluorescent protein), 9t, 12
- MAPs. *See* Microtubule-associated proteins (MAPs), GFP-tagged
- Materials properties, imaging techniques for measuring, 257–269
- MATLAB (software), 73t, 286, 287, 292, 313, 652
- Matrigel, 322, 458
- Maxwell's equations of electromagnetic waves, 676, 677
- mCherry (fluorescent protein), 9t, 12, 16, 17–18, 70, 207, 208f, 209f, 372, 606, 611
- Mean square displacement (MSD), 260, 264–266, 277
- Mechanical properties of cells and tissues, measuring, 257–269
- Mechanical stress, imaging live cells under, 641–658
 - analysis of cytoplasmic strain from endogenous intermediate filament networks, 652–654, 653f
 - analysis of intermediate filament displacement, 649–652, 650f
 - choosing a length scale for subcellular analysis, 650–651
 - computation of displacement index, 651–652
 - chambers for observation, 643–649
 - coverslip stability during force application, 643
 - deforming the endothelial surface using microneedles, 644
 - devices for application of substrate strain, 648–649
 - flow chambers for application of shear stress, 644
 - fluid dynamics considerations, 644–645, 646f
 - glass capillary tubes, 647–648
 - open chambers for access to the cell surface, 644
 - parallel plate flow chambers, 645–647
 - parallel plate flow chamber with physical access to the cells, 647, 647f, 648f
 - timing of transient transfection using green fluorescent protein fusion proteins, 643–644
- protocols, 655–657
 - coating coverslips with microspheres, 655–656
 - transfection and plating procedure for 4-cm coverslips, 657
- reasons for imaging, 641–642
 - relating to biomechanical models, 642
- Mello, Craig, 353
- Membrane systems and traffic, imaging, 623–638
 - construction and expression of organelle-targeted GFP-fusion proteins, 626–627
 - data analysis, 628–629
 - calculation of changes in protein concentration, 628–629
 - membrane movement, 628
 - imaging chamber setup, 625–626
 - instrumentation, 623–625
 - photoactivatable GFP, 628
 - photobleaching to highlight transport intermediates, 627–628, 627f
- protocols
 - activating photoactivatable proteins with laser light, 638
 - performing a time-lapse experiment, 633–635
 - photobleaching with CLSM, 636
 - photobleaching with older CLSM, 637
- reagents and protocols
 - actin-depolymerizing drugs, 630
 - aluminum fluoride, 630
 - ATP depletion, 630
 - brefeldin A, 629
 - colchicine, 629–630
 - drugs, 629–631
 - dyes, 631
 - fluorescent protein alternatives, 632
 - microtubule disruptors, 629–630, 629f
 - nocodazole, 629–630, 629f
 - protein synthesis inhibitors, 630
 - small interfering RNA (siRNA), 631
 - small-molecule compounds, 630–631
 - temperature blocks, 631
 - ts045 vesicular stomatitis glycoprotein-GFP, 631–632, 632f
- mEOS2 (fluorescent protein), 17
- mEOS (fluorescent protein), 70
- Mesentery preparation in mice and rats, 477t, 478, 478f, 497
- Metadata, 285

730 ■ INDEX

- MetaMorph (software), 73t, 289
Methotrexate, 547, 560
Microfluidic chips, 360–361
Microinjection
 into *Drosophila*, 392–393, 392f
 of fluorochrome-labeled intermediate filament proteins, 584, 597–598
 into mitotic mammalian cells, 577
Microlymphangiography, 503
Micropatterning cell–substrate adhesions, 43–51, 44f, 49f, 50f
Microrheology, 257–269
 active
 description, 259
 magnetic pulling, 258f
 magnetic twisting cytometry (MTC), 258f, 260–264
 magnetic twisting cytometry (MTC), 258f, 260–264
 calibration, 262
 cell types, 262
 data analysis, 262–263
 experimental requirements for, 260–262
 imaging, 262
 limitations of, 263–264
 magnetic beads, 260–261
 magnetic-field source, 261–262
 protocol, 268–269
 schematics, 261f
 particle tracking, 266–267
 image acquisition, 266–267
 image processing, 267
 linking, 267
 passive
 analysis of data, 266
 description, 258f, 260
 experimental requirements for, 265–266
 one-point, 264
 physical limitations on, 266
 two-point, 264–265
 rheology concepts, 258–259, 258f
 bulk rheology, 258, 258f
 linear viscoelasticity, 259
 nonlinear elasticity, 259
Microscope. *See also* Microscopy; *specific types of instruments*
 FRAP experiment setup, 70–73
 OMX, 203–214
 optics, 324–326
 aberrations that reduce signal-to-noise ratio, 325–326
 fluorescence filter sets, 325
 objective-lens correction, 325
 objective-lens magnification, 324–325
 objective-lens numerical aperture, 324
 Microscopy. *See also specific types*
 atomic force microscopy (AFM), 183–201
 fluorescence lifetime imaging microscopy (FLIM), 100–101, 101f, 112–113
 photoactivation localization microscopy, 213
 total internal reflection fluorescence and spinning-disk confocal (TIRF/SDC) microscope system, 119–138
 Microscopy medium (recipe), 536
 Microspheres
 coating coverslips with, 655–656
 coverslip stability and, 643
 preparing for AFM, 198–200, 199f
 Microtubule-associated proteins (MAPs), GFP-tagged
 construction of, 611–612
 examples of microtubule-binding protein fusion to fluorescent proteins, 608t–609t
 microscopy, 613–614
 overexpression, issues associated with, 614
 overview of, 610–611
 transfection of, 612–613
 Microtubule disruptors, 629–630, 629f
 Minimally invasive flow (MIF), 647, 647f, 648f
 Mirror. *See* Dichroic mirrors
 Mitogen-activated protein kinase (MAPK) pathway, 95
 Mitosis, tracking of, 249–250, 249f, 250f
 Mitotic shakeoff, 578
 MitoTracker, 631
 mKate (fluorescent protein), 13, 70
 mKate2 (fluorescent protein), 9t, 13
 mKikGR, 70
 mKusabira Orange (fluorescent protein), 9t, 11
 M9 medium (recipe), 366
 Molecular motors, single-molecule imaging of, 667–668
 purification and labeling of motor proteins, 667
 self-labeling genetic tags, 668
 Motion modeling, 276
 Mouse
 anesthesia, 425, 436–438, 447, 448, 453, 459
 intravital microscopy of normal and diseased tissues, 475–518
 tumor–stroma interactions, in vivo imaging of, 419–438
 vital signs monitoring, 436–438
 Mouse mammary tumor virus (MMTV) promoter, 444–445, 565–566
 Mowiol mounting medium (recipe), 117
 MPLSM. *See* Multiphoton laser-scanning microscopy (MPLSM)
 mPlum (fluorescent protein), 9t, 12, 70
 mRFP1 (fluorescent protein), 9t, 12
 mRuby (fluorescent protein), 9t, 12–13
 MSD (mean square displacement), 260, 264–266, 277
 MS2-GFP system, for RNA visualization and quantification
 components of, 698–699, 699f
 fluorescent tagging of MS2 protein, 701
 MS2-binding sites, 698–699, 699f, 700
 nuclear localization sequence (NLS), 698, 701
 promoters, 700
 quantifying RNA molecules in mRNA particles by measuring light output of RNA FISH probes, 706–710, 710f
 transfection of reporter mRNA and MS2-GFP plasmids, 701, 703–705
 use of, 699–700
 MS medium (recipe), 385
 MTC. *See* Magnetic twisting cytometry (MTC)
 MTFP1 (fluorescent protein), 9t, 10
 μManager (micro-manager), 289
 Multiphoton imaging, 395t, 401
 Multiphoton laser-scanning microscopy (MPLSM)
 detector noise, 323
 illumination and detection in, 328, 328f
 intravital microscopy in the mouse, 475, 480f, 481, 484, 484f
 extravascular parameters: interstitial diffusion, convection, and binding, 518
 vascular parameters: angiogenesis and hemodynamics, 508
 vascular parameters: leukocyte-endothelial interactions, 512–513
 vascular parameters: vascular permeability, 511
 Multiphoton microscopy
 advantages over confocal microscopy, 442–443, 443f
 animal models for multiphoton imaging, 444–448
 cell lines, 447
 mammary tumors, 447–448, 448f
 transgenic mice, 444–447, 445f, 446f
 cell behavior
 gene discovery based on, 456
 measurement in vivo, 456–457
 equipment, 448–451, 449f
 fluorophores for, 448–451, 450f, 451f
 imaging window, 452–455, 452f
 photoswitching, 453–455, 454f
 of tumors in vivo, 441–459
 animal models, 444–448
 collection needles, preparation and handling of, 458–459
 gene discovery based on behavioral analysis, 456
 intravital imaging at single-cell resolution, 442
 invasion and intravasation
 microenvironments, 446–447, 446f
 mammary-invasion window, 452–455, 452f
 measurement of cell behavior, 456–457
 stereotactic-imaging box, 453, 453f
 vasculature visualization, 451–452
 in vivo invasion assay, 455–456, 455f, 458–459
 Multiple-hypothesis tracking (MHT), trajectory construction and, 274–276
 Murine phosphoglycerate kinase promoter, 36
 Murine RNA polymerase II promoter, 36
 Muscovite mica, as substrate for AFM, 194, 195–196
 mWasabi (fluorescent protein), 9t, 10
- N
- National Institutes of Health (NIH) Image software, 443

- Navier–Stokes equations, 645, 648
 Nematodes. *See Caenorhabditis elegans*
 NES (nuclear export sequence), 525
 Neurons, imaging *Drosophila*, 413–415
 Neutral density filters, 326–327
 Nipkow disk, 129, 132, 154, 156, 420
 NIS-Elements (software), 289
 NLS (nuclear localization sequence), 698, 701
 Nocodazole, 578, 629–630, 629f
 Noise
 autofluorescence, 634
 charge-coupled device (CCD) camera,
 58–59, 62–63, 64, 342
 clock-induced charge, 62–63
 excess noise factor, 63
 Poisson, 59
 readout, 58–59, 62
 shot noise, 287
 signal-to-noise ratio, 53–54, 64–65
 sources, 323–324
 detector noise, 323
 illumination noise, 323
 Poisson or shot noise, 323–324
 stray light/spurious photons, 323–324
 thermal, 58, 62, 64
 Nonlinear elasticity, 259
 Nonlinear filters, 242, 243f
 Nonpixel data, 285
 Nuclear export sequence (NES), 525
 Nuclear localization sequence (NLS), 698, 701
 Numerical aperture, lens, 142, 324, 335, 336f,
 338–339
 digital scanned laser light sheet
 fluorescence microscopy
 (DSLM), 215, 223–224
 total internal reflection fluorescence
 (TIRF) microscopy, 661, 675,
 680, 680f, 682–683
 Nyquist frequency, 335, 342
- O**
- Objective lens
 choosing, 338–339, 398, 399t
 correction, 325
 fluorescence recovery after
 photobleaching (FRAP) and,
 71–73, 72f
 magnification, 324–325
 numerical aperture, 324
 total internal reflection fluorescence
 (TIRF) microscopy, 123–125,
 665
 OFDI (optical frequency domain imaging),
 481–482, 482f
 Offset, setting CCD camera, 65
 Oligo (software), 708
 OME Data Model, 286, 287
 OME Server, 294
 OME-TIFF, 287
 OME-XML, 286–287
 OMX (optical microscope experimental),
 203–214, 404
 components and layout, 205f
 features, 395t
 future directions, 211–213
 image processing for live cell imaging,
 212–213
 photoactivation localization
 microscopy, 213
 3D TIRF, 212
 TIRF (total internal reflection
 fluorescence), 212
 two-dimensional SI microscopy in
 living cells, 212
 history and design, 203–206
 imaging applications using, 206–211
 high temporal resolution analysis,
 207, 208f, 209f
 three-dimensional structural
 illumination microscopy (3D-
 SIM), 207–211, 210f, 211f
 imaging modalities, 404
 Open Microscopy Environment (OME), 286,
 294
 Open Microscopy Environment Remote
 Objects (OMERO), 294
 Optical frequency domain imaging (OFDI),
 481–482, 482f
 Optical-highlighter fluorescent proteins,
 13–14, 14t, 15f
 Optical microscope experimental. *See* OMX
 (optical microscope
 experimental)
 Optical sectioning
 confocal fluorescence microscopy, 222–223
 in light sheet-based fluorescence
 microscopy (LSFM), 215
 Optical sections, 174–175
 Orange fluorescent proteins, 9t, 11–12
 Organelle markers, imaging, 623, 624f
 Organelle-specific dyes, 631
 Origin (software), 313
 Overexpression, of GFP-tagged microtubule-
 associated proteins (MAPs), 614
- P**
- PAA (polyacrylamide), as blocking agent for
 micropatterning cell–substrate
 adhesions, 43–51, 44f, 49f
 PALM. *See* Photoactivated localization
 microscopy (PALM)
 Pancreatic window preparation in mice, 476,
 477t, 494
 Paraformaldehyde fixative solution 4%
 (recipe), 115
 Parallel plate flow chambers, 645–647
 with physical access to the cells, 647,
 647f, 648f
 Particle detection, computational image
 analysis and, 272, 273–274, 273f
 Particle localization, quantitative image
 analysis and, 245–246
 bottom-up approaches, 245–246
 top-up approaches, 246
 Particle tracking
 computational image analysis, 272–276
 motion modeling, 276
 particle detection, 272, 273–274, 273f
 trajectory construction, 272, 273f,
 274–276, 275f
 microrheology, 266–267
 image acquisition, 266–267
 image processing, 267
 linking, 267
 quantitative image analysis, 250–252
 deterministic approaches, 250–251,
 251f
 probabilistic approaches, 251–252, 252f
 PBS (recipe), 116, 602
 PCH (photon-counting histogram), 231
 Penetration depth, total internal reflection
 fluorescence (TIRF)
 microscopy, 676–678
 Peripherin, GFP-tagged, 586f
 Perutz, Max, 352
 Phase contrast, in passive microrheology, 265
 Phenolphthalein, 321
 pH indicators, 321
 pHLuorins, 28
 Phosphate-buffered saline 10× (recipe), 41,
 51, 201, 415
 Phosphoinositides, 523
 Phosphoribosylaminoimidazole, 343
 Phosphorylation, of EGF (epidermal growth
 factor) receptor, 97–101, 99f,
 101f, 103
 Phosphorylation biosensors, 28
 Photoactivatable fluorescent proteins, 14, 16,
 70
 Photoactivatable green fluorescent protein
 (PA-GFP), 14, 16, 70, 76f, 615,
 628
 Photoactivated localization microscopy
 (PALM), 120, 213, 404, 667
 fluorescence (F-PALM), 404
 single-particle-tracking (SPT-PALM), 404
 total internal reflection fluorescence
 (TIRF) microscopy, 668–670,
 669
 Photoactivation, with laser light, 638
 Photobleached images, acquisition of, 77
 Photobleaching. *See also* Fluorescence
 recovery after photobleaching
 (FRAP)
 camera exposure time and, 64
 cellular damage from, 80–81
 confocal laser-scanning microscopy
 (CLSM), 636–637
 confocal microscopy, 161–163, 162f,
 222–223
 digital scanned laser light sheet
 fluorescence microscopy
 (DSLM), 222–223
 fluorescence loss in photobleaching
 (FLIP), 68, 68f, 77, 78, 83
 fluorescent probes for, 69–70
 FRET acceptor, 98–99, 99f, 108–110
 to highlight transport intermediates,
 627–628
 in live cell imaging of yeast, 349
 reversibility, 79–80
 two-photon fluorescence microscopy,
 222–223
 in vivo imaging of tumor-stroma
 interactions, 431
 Photoconversion, fluorescent, 465, 467–468,
 468f, 469f, 472–474
 Photoconversion blocking buffer (recipe), 474
 Photoconvertible fluorescent proteins,
 16–17, 70
 Photodamage, in vivo imaging of
 mammalian cells and, 326–327

732 ■ INDEX

- Photolithography, 46–47
 Photon-counting histogram (PCH), 231
 Photons, spurious, 323–324
 Photoperturbation, 67–68, 68f, 77–78. *See also* Fluorescence recovery after photobleaching (FRAP)
 Photoresist, 43–50, 44f, 49f
 Photoshop, 290
 Photoswitchable fluorescent proteins, 17–18
 Phototoxicity
 in confocal microscopy, 161–163
 in imaging tagged chromosomes, 548–549, 549f
 in live cell imaging of yeast, 349
 in vivo imaging of tumor–stroma interactions, 431
 PIRE5 vector, 615
 Pixels, 284
 Plants, live cell imaging of, 371–385
 experimental design, 371–374
 Agrobacterium tumefaciens, transferring binary vector into, 373
 analysis, 374
 cloning strategies, 372–373
 data collection, 374
 fluorescent protein choice, 371–372
 fluorescent protein fusions, 372–373
 microscopes, 374
 preparing plant samples for, 374
 transgenic plant lines, generating, 373
 validating the fusion protein by rapid, transient expression, 373
 four-dimensional imaging of plant cells during cell cycle (protocol), 380–385
 discussion, 385
 four-dimensional data collection and processing, 383, 384f
 materials, 380–381
 plant tissue preparation, 382
 recipes, 384–385
 root-growth chamber preparation, 382, 383f
 three-dimensional data collection and processing, 382–383
 transfer of vectors into *Agrobacterium* strain GV3101, 381
 transformation and cotransformation of *Arabidopsis* by flower dip, 381–382
 transient expression of fusions in tobacco, 381
 troubleshooting, 383–384
 vector construction, 381
 imaging assay for plant protein–protein interactions (protocol), 375–379
 discussion, 375–379, 378–379
 materials, 375–376
 microscope assay, 378, 379f
 plant infiltration and coinfiltration, 377–378, 377f
 preparation of *Agrobacterium* competent cells, 376
 preparation of split YFP vectors, 376
 transfer binary vectors into *A. tumefaciens* strain GV3101, 376–377
 troubleshooting, 378
 protocols, 375–385
 four-dimensional imaging of plant cells during cell cycle, 380–385
 imaging assay for plant protein–protein interactions, 375–379
 Plus-end tracking proteins (+TIPS), 610–611, 614
 Point-spread function (PSF), 141–145, 141f, 143f, 148–149, 163, 165, 223–224, 242–243, 702
 description of, 334–335
 experimental determination of, 348–349
 impulse response of microscope, 334
 particle detection and, 273–274
 shape, 347
 spherical aberration, 334–335, 347, 348f
 total internal reflection fluorescence (TIRF) microscopy, 667
 Poisson noise, 59, 323–324
 Polyacrylamide (PAA), as blocking agent for micropatterning cell–substrate adhesions, 43–51, 44f, 49f, 50f
 Poly-D-lysine coverslips, preparation and use of, 626
 Poly-L-lysine coverslips, preparation and use of, 365–366
 Polystyrene particles, as probes for passive microrheology, 265
 Population score, 307
 PostgreSQL database, 294
 Posttranslational modifications, 95–96, 102
 Probe, for atomic force microscopy, 185
 Promoters
 actin, 36
 cytomegalovirus, 36, 612, 700
 for expression of fluorescent protein fusions in plants, 372–373
 inducible, 612
 mouse mammary tumor virus *MMTV*, 444–445, 565–566
 for MS2-GFP protein expression, 700
 murine phosphoglycerate kinase, 36
 murine RNA polymerase II, 36
 in plants, 372–373
 ribosomal L30, 700
 RNA-Pol II large subunit, 700
 simian virus-40 (SV40), 36
 SV2, 36
 tetracycline, 612
 Protease-cleavage assay, 28
 Protein
 functionality assays, 41
 synthesis inhibitors, 630
 Protein fusions, fluorescent. *See* Fluorescent protein fusions (FPFs)
 Protein interactions
 bimolecular fluorescence complementation (BiFC) assay for plant protein–protein interactions, 375–379
 measuring by fluorescence cross-correlation spectroscopy (FCCS), 101–102, 114–115
 measuring by FRET (*See* Fluorescence resonance energy transfer (FRET))
 microscopy schemes for study of, 96–97, 96f
 signaling networks, 95, 102
 PS-CFP2 (fluorescent protein), 16
 Pseudocolor lookup table, 167
 PSF. *See* Point-spread function (PSF)
 PtK cells, 572–573, 573t, 574f
 Pulse oximeter, 436
 Puromycin, 630
- ## Q
- Qdots. *See* Quantum dots
 Quantitative image analysis, 239–254
 cell tracking
 deformable models, 248–249
 deterministic two-step approaches, 248
 mitosis handling, 249–250, 249f, 250f
 probabilistic approaches, 249
 classification, 240, 240f, 252–253
 computational analysis, why to use, 271–272
 completeness, 272
 consistency, 272
 efficiency, 271–272
 computational methods, 241–253
 image preprocessing, 240, 240f, 241–243, 242f
 deconvolution, 242–243
 denoising, 241–242, 243f
 particle localization, 245–246
 bottom-up approaches, 245–246
 top-up approaches, 246
 particle tracking, 250–252
 deterministic approaches, 250–251, 251f
 probabilistic approaches, 251–252, 252f
 registration, 240, 240f, 246–247, 248f
 segmentation, 240, 240f, 243–245
 deformable models and, 245
 edge-based, 244
 region-based, 244–245
 threshold-based, 243–244, 244f
 system biology and, 253
 tracking and motion analysis, 240, 240f, 247
 cell tracking, 248–250, 249f, 250f
 particle tracking, 250–252, 251f
 workflow for, 240–241, 240f
 Quantum dots, 452, 463, 659, 668, 671f
 Quantum efficiency, CCD camera, 57, 57f
 Quenching solution (recipe), 537
- ## R
- R (software), 313
 Rabbit ear chambers, 476f, 477t, 488–489
 Rabbits
 corneal pocket assay in rabbits, 477t, 479, 479f, 500
 ear chambers, 476f, 477t, 488–489
 Rasband, Wayne, 291
 Ras reporter, 565–566
 Rayleigh criterion, 120, 142, 143f, 335, 335f
 React buffer 2 (recipe), 561
 Readout noise, 58–59, 62
 ReAsH (biarsenical reagent), 464, 467–468, 468f, 469f, 470, 632

- ReAsH-EDT2, 41
- Recipes
- activated sodium orthovanadate, 116
 - assembly buffer, 600
 - ATV solution, 200–201
 - bind-silane working solution, 51
 - calcium- and magnesium-free phosphate-buffered saline (CMF-PBS), 562
 - column buffer, 600
 - column buffer for inclusion bodies, 601
 - detergent buffer, 601
 - DFCS culture medium, 201
 - dialysis buffer, 602
 - dialysis buffer for inclusion bodies, 601
 - disassembly buffer, 602
 - DMF, 115
 - Dulbecco's PBS, 536
 - ECM coating solution, 51
 - egg salts solution, 366
 - extraction buffer, 600
 - germination plates, 385
 - HEPES buffer, 537
 - homogenization buffer, 601
 - homogenization buffer for inclusion bodies, 601
 - imaging buffer, 538
 - imaging medium, 638
 - LB liquid medium, 561
 - LB plates, 561
 - lipid mix A, 537
 - lipid mix B, 538
 - Luria-Bertani (LB) liquid medium, 384–385
 - microscopy medium, 536
 - M9 medium, 366
 - Mowiol mounting medium, 117
 - MS medium, 385
 - paraformaldehyde fixative solution (4%), 115
 - PBS, 116, 602
 - phosphate-buffered saline (10x), 41, 51, 201, 415
 - photoconversion blocking buffer, 474
 - quenching solution, 537
 - react buffer 2, 561
 - selection plates, 385
 - sephadex column buffer, 602
 - SOC medium, 561
 - Sorensen's phosphate buffer, 201
 - staining mix A, 537
 - staining mix B, 538
 - staining mix C, 538
 - TE buffer, 562
 - TNE, 601
 - TR buffer, 562
 - Tris-Cl, 116
 - Valap, 582
 - wash buffer, 601
- Red fluorescent protein (RFP), 9t, 12–13
- Refractive index, 335, 347–349, 675, 676–677, 677t
- Region growing, 244–245
- Registration, image analysis and, 240, 240f, 246–247, 248f
- Resolution, 54, 57–58, 334–336
- Rayleigh criterion, 120, 142, 143f, 335, 335f
 - spatial, 335
 - high-content screening in mammalian cells, 305
 - temporal, 335–336
 - acquisition speed, 304–305
 - autofocus speed, 305
 - filter and shutter times, 305
 - high-content screening in mammalian cells, 304–305
 - sample number, 305
 - sample preparation, 305
 - stage-movement speed, 305
- Resolution test target, 170, 170f, 173
- Resolving power
- contrast-transfer function (CTF) and, 142
 - point-spread function (PSF) and, 141–142
 - Rayleigh criterion, 142, 143f
- Restoration techniques, 290
- Reynolds number, 645, 646
- RFP. *See* Red fluorescent protein (RFP)
- Rheology, 258–259, 258f. *See also* Microrheology
- Rhodamine-transferrin, 631
- Ribosomal L30 promoter, 700
- RNA, visualization and quantification in living cells, 697–711
- fluorescent in situ hybridization (FISH), 697, 702, 706–710
 - fluorescent in vivo hybridization (FIVH), 697–698
- method steps
- Step 1: construction of reporter mRNA containing the repeats of MS2-binding sites, 700
 - Step 2: construction of MS2-GFP plasmid, 700–701
 - Step 3: coexpression of the reporter RNA and MS2-GFP-binding protein and visualization of mRNPs, 701
 - Step 4: quantification of number of RNA molecules in each mRNAP, 702
- MS2-GFP system
- components of, 698–699, 699f
 - fluorescent tagging of MS2 protein, 701
 - MS2-binding sites, 698–699, 699f, 700
 - nuclear localization sequence (NLS), 698, 701
 - promoters, 700
 - transfection of reporter mRNA and MS2-GFP plasmids, 701, 703–705
 - use of, 699–700
- protocols
- quantifying RNA molecules in mRNA particles by measuring light output of RNA FISH probes, 706–710, 710f
 - transfection of plasmids and imaging RNA molecules in living cells, 703–705
- RNA FISH, 702, 706–710
- RNA interference (RNAi), 301, 318, 351, 402, 572, 614
- RNA-Pol II large subunit promoter, 700
- Rolling ball filtering, 244
- Root-growth chamber, preparation of, 382, 383f
- Rose chamber, 576–577, 581, 581f, 613, 689
- rsCherry (fluorescent protein), 18
- rsCherryRev (fluorescent protein), 18
- Russ, John, 290
- ## S
- Saccharomyces cerevisiae*. *See also* Yeast, live cell imaging in
- actin-GFP protein fusion expression in, 36
 - light sensitivity, 334
 - size, 334
- Scientific Image DataBase (SIDB), 294
- SDC. *See* Spinning-disk confocal (SDC) microscopy
- Second harmonic generation, 442–443, 484, 486
- Secretory pathway and associated organelles, 624f
- Sedat, John, 203, 206
- Segmentation, image, 240, 240f, 243–245
- deformable models and, 245
 - edge-based, 244
 - region-based, 244–245
 - threshold-based, 243–244, 244f
- Selection plates (recipe), 385
- Sephadex column buffer (recipe), 602
- Shear modulus, 258f, 259
- Shear stress, 642, 644, 645, 649
- Short-hairpin RNA (shRNA), 301
- Shot noise, 287, 323–324
- SIDB (Scientific Image DataBase), 294
- Signaling networks, 95, 102
- Signal-to-noise ratio
- aberrations that reduce, 325
 - binning, effect of, 65
 - calculating, 177
 - camera exposure time and, 64
 - confocal microscopy and, 163, 164f, 165, 167, 177–179, 178f
 - data acquisition and, 287
 - deconvolution of images and, 144, 146–148, 290
 - defined, 53–54
 - dependence of localization error and resolution on, 337, 337f
 - information capacity and, 336–337
 - optimized fluorescent images and, 276, 277f, 278
 - total internal reflection fluorescence (TIRF) microscopy, 667
- Simian virus-40 (SV40) promoter, 36
- Simulation-based benchmarking, 279
- Single-molecule imaging
- future of, 670
 - of molecular motors, 667–668
 - photoactivated localization microscopy (PALM), 668–670, 669
- protocol
- determining single-molecule intensity as a function of power density, 671–672, 671f
 - motility assay, 673–674
- stochastic optical reconstruction microscopy (STORM), 668–670, 669

734 ■ INDEX

- Single-molecule imaging (*continued*)
 total internal reflection fluorescence (TIRF) microscopy, 659–674
 peripherals for, 663–667
 data analysis, 66f, 666–667
 dichroic mirrors, 664–665
 filters, 664–665
 illumination source, 663–664
 objectives, 665
 setup, 661–663
 adjustment of incident angle, 662–663
 commercially available systems, 661
 laser alignment, 661–662, 662f
 theory of, 659–660
- Single-particle-tracking photoactivated localization microscopy (SPT-PALM), 404
- Single-photon microscopy, for intravital microscopy in the mouse
 extravascular parameters: interstitial diffusion, convection, and binding, 517
 vascular parameters: angiogenesis and hemodynamics, 507–508
 vascular parameters: leukocyte-endothelial interactions, 512
 vascular parameters: vascular permeability, 510
- Single plane illumination microscopy (SPIM), 220–222–225, 227, 403
- Site-directed mutagenesis, 606
- SlideBook (software), 289
- Slide holder, thermally regulated, 346–347, 346f
- Small interfering RNA (siRNA), 300–302, 318, 606, 631
- SNAP tag, 668, 670
- Snell's law, 660, 676, 676f
- SOC medium (recipe), 561
- Software tools, 283–295
 for analysis, 291–293
 for data acquisition, 287–289
 for digital images, 284–287
 for high-content screening microscopy, 312–313, 313t
 for image data management, 293–294
 for image processing, 290–291
- SoftWoRx (software), 702
- Sorensen's phosphate buffer (recipe), 201
- Sorger, Peter, 294
- Spatial resolution, 335
 high-content screening in mammalian cells, 305
- Spherical aberration
 causes, 148
 in confocal microscopy, 165, 165f
 correcting, 334–335
 motorized correction lenses, 403
 description, 175–176
 imaging thick *Drosophila* specimens and, 400–401
 point-spread function and, 334–335, 347, 348f
- SPIM (single plane illumination microscopy), 220–222–225, 227, 395t
- Spinning-disk confocal (SDC) microscopy illumination and detection in, 328, 328f
- total internal reflection fluorescence and spinning-disk confocal (TIRF/SDC) microscope system, 119–138
- total internal reflection fluorescence microscope (TIRFM)
 compared, 678, 678t
- tubulin and microtubule-associated proteins (MAPs), 613–614
- for in vivo imaging of tumor–stroma interactions, 420, 421f, 424f, 426–431
- SPR-220 (photoresist), 43–49, 44f, 49f
- SPT-PALM. *See* Single-particle-tracking photoactivated localization microscopy
- StackReg (software), 73t
- Staining mix A (recipe), 537
- Staining mix B (recipe), 537
- Staining mix C (recipe), 537
- STED (stimulated emission depletion), 395t, 403, 404
- Stelzer, Ernst, 403
- Stereotactic-imaging box, 453, 453f
- Stochastic optical reconstruction microscopy (STORM), 667, 668–670, 669f
- Stokes–Einstein relation, 264
- Stokes shift, 13, 340
- STORM (stochastic optical reconstruction microscopy), 667, 668–670, 669f
- Strain, 258–259, 258f
- Stray light/spurious photons, 323–324
- Stress, 258–259, 258f
 mechanical stress, imaging live cells under, 641–658
- Stress-to-strain ratio, 186
- Structured illumination methods, 172–174, 174f, 404
- Stuurman, Nico, 294
- Sulston, John, 352
- Superfolder GFP (fluorescent protein), 9t, 16
- Support vector machines (SVMs), 311
- SVMs (support vector machines), 311
- SV2 promoter, 36
- System biology, quantitative image analysis and, 253
- SYTO 14 dye, 608
- ## T
- TagBFP (fluorescent protein), 7, 9t
- Tagged Image File Format (TIFF), 287
- TagGFP (fluorescent protein), 10
- TagRFP (fluorescent protein), 9t, 11, 13, 70
- Tail lymphatics in mice, 477t, 479f, 502–503
- Tau, 610
- tdEos (fluorescent protein), 17
- tdTomato (fluorescent protein), 9t, 11, 70
- TE buffer (recipe), 562
- Temporal resolution, 335–336
 high-content screening in mammalian cells, 304–305
 acquisition speed, 304–305
 autofocus speed, 305
 filter and shutter times, 305
 sample number, 305
 sample preparation, 305
- stage-movement speed, 305
- Tetracycline inducible or repressible promoters, 612
- Tetracycline response element (TRE), 567, 567f
- Tetracysteine tag, 41
- Tetracysteine-tagged proteins, 463–465, 467–468, 468f, 469f, 470–471, 632
- Texas red dextran, 451–451
- TFI (total fluorescence intensity), 702, 709–710
- Thermal noise, 58, 62, 64
- Theta imaging, 395t
- Thick specimens, imaging
 difficulties in imaging, 139
 method of imaging
 choosing a method, 139–140, 178–179
 confocal microscopy, 151–172
 deconvolution, 140–150
 structured illumination, 172–174
 results, 174–180
 chromatic aberration, 176, 176f
 signal-to-noise ratio, 177–178
 spherical aberration, 175–176
 three-dimensional reconstruction, 179–180
- Thomas, Charles, 356
- Thompson, Mike, 356
- Three-dimensional structural illumination microscopy (3D-SIM), 204, 207–211
 for high spatial resolution analysis, 207–208, 210f, 211f
 sample preparation and imaging protocols for, 208–211
- Thymidine, 578
- TIFF (Tagged Image File Format), 287
- Time-lapse images, 284
Caenorhabditis elegans live cell imaging, 356
Drosophila live cell imaging, 388
 experiment protocol for confocal laser-scanning microscopy (CLSM), 633–635
 fluorescence recovery after photobleaching (FRAP), 81–83
 background subtraction, 82, 82f
 corrections, 82–83, 82f
 image alignment, 81–82
 normalization, 82f, 83
 photobleaching, 82, 82f
 steps in image analysis, 82f
 high-content screening microscopy, 307, 308f
 movie acquisition, total internal reflection fluorescence (TIRF) microscopy and, 690
- Time series, 311
- TIRF (total internal reflection fluorescence). *See also* Total internal reflection fluorescence and spinning-disk confocal (TIRF/SDC) microscope system; Total internal reflection fluorescence (TIRF) microscopy
 OMX microscopy, 212
 3D, 212

- TNE (recipe), 601
Tobacco, infiltration of leaves, 377–378, 377f, 381
Tomato (fluorescent protein), 450–451, 451f
Topaz (fluorescent protein), 9t, 11
Total fluorescence intensity (TFI), 702, 709–710
Total internal reflection fluorescence and spinning-disk confocal (TIRF/SDC) microscope system, 119–138
analysis, 136
applications, examples of, 136, 137f, 138
components, 122f, 123f, 124t
condenser, 125
design criteria, 120
digital cameras, 133–135
environmental control, 135–136
specimen positional control, 135–136
temperature control, 135
vibration reduction, 136
epi-illumination, 125–133
excitation/emission filters and dichromatic mirrors, 127t, 132–133
Koehler wide-field epi-illuminator, 125–128
laser merge module, 131–132, 131t
SDC scanner, 129–131, 130f
TIRF epi-illuminator, 128–129
hardware automation, 136
image acquisition, 136
microscope, 121–122
objective lenses, 123–125
overview of system, 120–121
transillumination, 125
Total internal reflection fluorescence (TIRF) microscopy
alignment, 686–687, 687f
applications, 691–692
imaging cytoskeleton dynamics, 691, 693f
imaging exo- and endocytosis, 691–692, 694f
calibration, 687–688
combining with other imaging modalities, 683–684
confocal microscopy compared, 678, 678t
critical angle, 676, 676f
instrumentation
cameras, 679, 683
fluorescent filter cubes, 682
high NA objective lenses, 682–683
illumination light, 680–681, 680f
intermediate optics (TIRF illuminators), 682
lasers, 680–681, 680f
overview, 679–680, 680f
temperature-controlled box, 683
lipid imaging in living cells, 527, 527f
molecular motors, single-molecule imaging of, 667–668
objective-type, 679, 679t, 680, 680f, 682
optical principles, 676–679
penetration depth, 676–678
peripherals for, 663–667
data analysis, 666–667, 666f
dichroic mirrors, 664–665
filters, 664–665
illumination source, 663–664
objectives, 665
prism-type, 679, 679t
protocol
alignment and calibration, 685–688, 687f
quantitative analysis, 692, 693f, 694, 694f
sample preparation for live cell imaging, 689–690
fluorescently labeling strategies, 689
imaging media solution, 690
live cell imaging chambers, 689
setup, 661–663
adjustment of incident angle, 662–663
commercially available systems, 661
laser alignment, 661–662, 662f
single-molecule imaging, 659–674
determining intensity as a function of
power density (protocol), 671–672, 671f
future of, 670
of molecular motors, 667–668
motility assay (protocol), 673–674
photoactivated localization microscopy (PALM), 668–670, 669
stochastic optical reconstruction microscopy (STORM), 668–670, 669
Snell's law, 676, 676f
structured illumination and, 404
theory of, 659–660, 676–679
time-lapse movies, acquisition of, 690
Total internal reflection fluorescent speckle microscopy (TIR-FSM), 119
Toxoplasma gondii, 147f, 150f, 164f, 168f
Tracking and motion analysis, 240, 240f, 247
cell tracking, 248–250, 249f, 250f
particle tracking, 250–252, 251f
Trajectory construction, computational
image analysis and, 272, 273f, 274–276, 275f
global-nearest-neighbor (GNN) algorithm, 274, 275
local-nearest-neighbor (LNN) algorithm, 274, 275f
multiple-hypothesis tracking (MHT), 274–276
Transfection
calcium phosphate-mediated, 546, 557
with DNA encoding a visible fluorescent protein (VFP)-tagged lipid-binding domain, 531–532
with GFP-tagged vimentin, 599–600
MS2-GFP system, 701, 703–705
protocol for transfection, 38–41
with tetracycline-tagged proteins, 464
timing of transient transfection using green fluorescent protein fusion proteins, 643–644
tubulin and microtubule-associated proteins (MAPs), 612–613
in vivo imaging of cells, 318
Transformation, calcium phosphate, 557
Transformation-rescue experiments, in *Caenorhabditis elegans*, 353
Transgenic mice, as animal models for multiphoton imaging, 444–447, 445f, 446f
Transistor-transistor logic (TTL) gating, 681, 684
Transposition, of Tn5 transposon with 256mer *lac* operator repeat and kan/neo selectable marker into BAC DNA, 552–555
TR buffer (recipe), 562
TRE (tetracycline response element), 567, 567f
Tris-Cl (recipe), 116
TRITC (tetramethyl rhodamine isothiocyanate) filter set, 11
T-Sapphire (fluorescent protein), 13
Tubulin, GFP-tagged
construction of, 611–612
examples of tubulin fusion to fluorescent proteins, 607t
history of, 610
microscopy, 613–614
overview, 610
permanent cell lines for expression of, 613, 615–617
transfection of, 612–613
Tumors, multiphoton imaging of, 441–459
advantages of multiphoton microscopy over confocal microscopy, 442–443, 443f
animal models, 444–448
collection needles, preparation and handling of, 458–459
gene discovery based on behavioral analysis, 456
intravital imaging at single-cell resolution, 442
invasion and intravasation microenvironments, 446–447, 446f
mammary-invasion window, 452–455, 452f
measurement of cell behavior, 456–457
microscopy equipment, 448–451, 449f
stereotactic-imaging box, 453, 453f
vasculature visualization, 451–452
in vivo invasion assay, 455–456, 455f, 458–459
Tumor-stroma interactions, in vivo imaging of, 419–438
anesthesia, long-term, 425
emission selection, 429–430
fast image collection to minimize motion artifacts, 427–428
flexible multicolor excitation, 428–429
fluorescent labeling of tumor components, 423
imaging several tumor regions in same mouse, 422–423
inverted or upright microscope selection, 426–427
microscope system selection, 426
minimally invasive access to tissue, 423–424
mouse care on microscope stage, 425–426
multiple tumor microenvironments in same mouse
analysis of, 422, 422f
generation of, 420
myeloid cell migration, 427f, 428f

736 ■ INDEX

- Tumor–stroma interactions, *in vivo* imaging
of (*continued*)
objective lenses, 430
photobleaching, 428f, 431
protocols, 432–438
 monitoring of vital signs for long-term survival under anesthesia, 436–438
 preparation of mice for long-term intravital imaging of mammary gland, 432–435, 434f
spinning-disk confocal (SDC) microscopy, 420, 421f, 424f, 426–431
technical barriers, resolving, 420–431
vascular leakage, dynamics of, 429f
x-y stage, 430
- Two-photon fluorescence microscopy
dynamic range, 225
illumination efficiency, 222
imaging speed, 225
lateral and axial extents of point-spread function, 223–224
photobleaching, 222–223
- U
- Unsupervised learning, 307
- Urethane, 425
- V
- Valap (recipe), 582
- Van Beneden, Edouard, 351
- Vascular endothelial growth factor (VEGF), 486, 487
- Vasculature visualization, tumor, 451–452
- Vectors
bacterial artificial chromosome (BAC), 542–543, 546, 552–555, 614
commercial, 612
for fluorescent protein fusions, 35–36
 in plants, 373, 376, 381
pIRES, 615
- Venus (fluorescent protein), 9t, 11
- Vesicular stomatitis glycoprotein-GFP, 631–632, 632f
- Video microscopy, for live imaging of *Caenorhabditis elegans*, 355–356
- VIGRA, 313
- Vimentin, 583, 584
analysis of displacement, 649–650, 650f
CFP labeled, 587, 587f
characterization of GFP-tagged, 585, 586f
construction and expression of GFP-tagged, 585
FRAP analyses of, 587f
microinjection of X-rhodamine vimentin, 597–598
purification
 of bacterially expressed vimentin, 593–594
 of bovine vimentin, 591–592
recovery of fluorescence in a living cell, 585f
transfection of cells with GFP-tagged, 599–600
 X-rhodamine labeling of, 595–596
- Viosensor fluorescent proteins, 26–29
- Virtual Cell (software), 73t
- Viscoelasticity, linear, 259
- Viscoelastic modulus, 258f, 260, 261f, 263, 265
- Viscoelastic response of cells, measuring, 259–269
- Viscous modulus, 258f, 259, 261f, 266
- Visible fluorescent protein (VFP)-tagged lipid-binding domains, 524–526
- Volocity (software), 289, 457
- W
- Wash buffer (recipe), 601
- Watershed transform, 244–245
- WEKA (software), 313
- Wheelock, Margaret, 37
- White, John, 352
- Wide-field microscopy. *See also specific applications*
axial resolution, 169f
confocal microscopy compared, 152f, 153f, 169f, 178f
deconvolution, 144–148, 395t
features, 395t
illumination and detection in, 328f
lipid imaging in living cells, 526
noise levels, 327
- Winoto, Lukman, 204
- X
- XML (Extensible Markup Language), 286–287
- X-rhodamine
labeling of vimentin, 595–596
microinjection of vimentin, 597–598
- Y
- Yeast, live cell imaging in, 333–350
brightness, 337–342
 camera setup, 341–342
 choosing an objective, 338–339
 dichroic mirrors, 339, 340
 filters, 339–340, 339f, 340f
 future developments in, 349–350
 image information capacity, 336–337
 instrumentation, 345–349
 environmental control devices, 345–346, 345–347
 experimental determination of point spread function, 348–349
 limiting geometric aberrations, 347, 348f
 refractive index matching using immersion media, 347–349
 thermally regulated slide holder, 346–347, 346f
photodamage, 349
resolution, 334–336
sample preparation and mounting, 343–345
 slide preparation, 343–345
 strain choice, 343
slide preparation, 343–345, 343f, 344f
 agarose cushion, 343–345, 344f
 mounting cells, 345
- Yellow fluorescent protein (YFP)
for imaging gene expression in living cells, 567–568, 567f, 569f
split vectors, 376
- Young's modulus, 186
- Z
- Zebra highlighter pen, 686
- ZsGreen (fluorescent protein), 10, 612